2018

INTELLIGENT UAV SCOUTING FOR FIELD CONDITION MONITORING

Hasan Seyyedhasani
University of Kentucky, hshasani@yahoo.com
Digital Object Identifier: https://doi.org/10.13023/ETD.2018.027

STUDENT AGREEMENT:

I represent that my thesis or dissertation and abstract are my original work. Proper attribution has been given to all outside sources. I understand that I am solely responsible for obtaining any needed copyright permissions. I have obtained needed written permission statement(s) from the owner(s) of each third-party copyrighted matter to be included in my work, allowing electronic distribution (if such use is not permitted by the fair use doctrine) which will be submitted to UKnowledge as Additional File.

I hereby grant to The University of Kentucky and its agents the irrevocable, non-exclusive, and royalty-free license to archive and make accessible my work in whole or in part in all forms of media, now or hereafter known. I agree that the document mentioned above may be made available immediately for worldwide access unless an embargo applies.

I retain all other ownership rights to the copyright of my work. I also retain the right to use in future works (such as articles or books) all or part of my work. I understand that I am free to register the copyright to my work.

REVIEW, APPROVAL AND ACCEPTANCE

The document mentioned above has been reviewed and accepted by the student's advisor, on behalf of the advisory committee, and by the Director of Graduate Studies (DGS), on behalf of the program; we verify that this is the final, approved version of the student's thesis including all changes required by the advisory committee. The undersigned agree to abide by the statements above.

Hasan Seyyedhasani, Student

Dr. Henry G. Dietz, Major Professor

Dr. Cai-Cheng Lu, Director of Graduate Studies

INTELLIGENT UAV SCOUTING FOR FIELD CONDITION MONITORING

Thesis

A thesis submitted in partial fulfillment of the requirements for the degree of Master of Science in Electrical Engineering in the College of Engineering at the University of Kentucky

By
Hasan Seyyedhasani

Lexington, Kentucky

Director: Dr. Henry G. Dietz, Professor of Electrical and Computer Engineering

Lexington, Kentucky

2017

ABSTRACT OF THESIS

INTELLIGENT UAV SCOUTING FOR FIELD CONDITION MONITORING

Precision agriculture requires detailed and timely information about field condition. In less than the short flight time a UAV (Unmanned Aerial Vehicle) can provide, an entire field can be scanned at the highest allowed altitude. The resulting NDVI (Normalized Difference Vegetation Index) imagery can then be used to classify each point in the field using a FIS (Fuzzy Inference System). This identifies areas that are expected to be similar, but only closer inspection can quantify and diagnose crop properties. In the remaining flight time, the goal is to scout a set of representative points maximizing the quality of actionable information about the field condition. This quality is defined by two new metrics: the average sampling probability (ASP) and the total scouting luminance (TSL). In simulations, the scouting flight plan created using a GA (Genetic Algorithm) significantly outperformed plans created by grid sampling or human experts, obtaining over 99% ASP while improving TSL by an average of 285%.

KEYWORDS: Unmanned Aerial Vehicle, Scouting, Fuzzy Inference System, Average Sampling Probability, Total Scouting Luminance, Genetic Algorithm

Hasan Seyyedhasani
October 20, 2017

INTELLIGENT UAV SCOUTING FOR FIELD CONDITION MONITORING

By

Hasan Seyyedhasani

Dr. Henry G. Dietz
Director of Thesis

Dr. Cai-Cheng Lu
Director of Graduate Studies

October 20, 2017

To my wife Paria, and parents, I could not have done it without you.
Thanks for all the love and support along the way …

&

To …

ACKNOWLEDGMENTS

I would like to thank my advisor Dr. Henry G. Dietz for his support, guidance, and mentorship throughout my research. I would also like to extend my gratitude to the remaining members of my graduate committee, Dr. Lump, Dr. Thapliyal, and Dr. Dvorak, for their continued input and feedback.

Finally, I would like to thank my family for their encouragement through these challenging years. I am indebted to my parents for their continual support and sacrifice throughout my early academic career, as well as, the confidence afforded to me during my time spent at the University of Kentucky. I am extremely appreciative of my wonderful wife, Paria, for her patience, perseverance, grace and hopeful disposition over these years. Her support has been critical in my academic success. I could not have made it through this program without the support of everyone mentioned here and certainly not without God.

TABLE OF CONTENTS

LIST OF TABLES

LIST OF FIGURES

CHAPTER 1: INTELLIGENT UAV SCOUTING FOR FIELD CONDITION MONITORING

1.1 SUMMERY

Precision agriculture requires detailed and timely information about field condition. In less than the short flight time a UAV (Unmanned Aerial Vehicle) can provide, an entire field can be scanned at the highest allowed altitude. The resulting NDVI (Normalized Difference Vegetation Index) imagery can then be used to classify each point in the field using a FIS (Fuzzy Inference System). This identifies areas that are expected to be similar, but only closer inspection can quantify and diagnose crop properties. In the remaining flight time, the goal is to scout a set of representative points maximizing the quality of actionable information about the field condition. This quality is defined by two new metrics: the average sampling probability (ASP) and the total scouting luminance (TSL). In simulations, the scouting flight plan created using a GA (Genetic Algorithm) significantly outperformed plans created by grid sampling or human experts, obtaining over 99% ASP while improving TSL by an average of 285%.

1.2 INTRODUCTION

Precision agriculture is receiving ever-increasing attention (Pierpaoli, Carli, Pignatti, Canavari, 2013) and is used for the assessment of inter- and intra-field spatial/temporal variations. Obtaining knowledge as to the various regions of a field such as crop growth status (Yu et al., 2013) is an important parameter that necessitates field monitoring. This shall allow the performance of the agricultural services, such as fertilizing, irrigation, insect and disease control, or logistics, in a proper, efficient time. Although remote sensing using satellites and aerial imagery have been used for monitoring the field condition (Hunt, Cavigelli, Daughtry, Mcmurtrey, Walthall, 2005; Yang, Everitt, Bradford, 2006; Inman, Khosla, Reich, Westfall, 2008), it brings up a number of issues. The information provided can only be utilized to evaluate the seasonal changes (long-term changes) of the crop growth, and is more suitable for large-scale analysis (Sakamoto et al., 2012; Zhang & Kovacs, 2012). Camera based observations, via UAV (Unmanned Aerial Vehicle), appears a viable solution to overcome the deficiencies associated with traditional methods of remote sensing (Miller, Adkins, Tully, 2017). Over

the last decade, the use of air-borne remote sensing has drastically increased in agriculture as it provides superior spatial/temporal flexibility and higher resolution images.

Application of the remote sensing allows farmers to collect actionable information with regard to different zones of their field. For instance, envision solely a section of a field necessitates irrigating, spraying, or fertilizing, one can thus save both time and money by addressing the site-specific needs. To that end, remote sensing and geographical information systems (GIS) are relying on color classification (Wharton et al., 1988; Wu, 2000) of the imagery captured from a field, following the coverage of the field. This stems from the promising results of the spectral vegetation indices such as NDVI (normalized difference vegetation index). The NDVI has proven to be useful in providing information with respect to different characteristics of the various regions of a field such as water-stressed regions and grown crops regions (Peñuelas, Gamon, Fredeen, Merino, Field, 1994). This happens via the classification of a field into a variety of colors, representing zones with specific characteristics. However, the relatively short flight time provided by the commercial UAVs doesn't allow either covering the entire field or obtaining high quality information of the field. The escalation of flight altitude (expansion of the camera's field of view) can make the field's complete coverage possible. Yet, the problem of lacking qualitative information due to low resolution of footage appears. As such, further and closer inspection is needed to better quantify or diagnose, such as the amount of spray application or irrigation for a specific region (Ehmke, 2013). Re-flight at lower altitude over a number of representative points of each color zone can provide high quality, actionable information as to the corresponding region.

A flight plan over a set of representative points conventionally takes place through human-directed frameworks. For instance, a farmer divides up the field, like a grid, and routes the vehicle to visit the intersections as distinct points. Although the method allows setting the representative points deterministically, it is unknown which field condition each intersection evidences. Another approach is that a human expert picks a number of representative points and routes the vehicle. The method, however, requires either the UAV landing or hovering around, following the completion of the

coverage flight, until the operator specifies the points relevant to the different field conditions. Both these methods have the issue of efficient sampling and routing. This is not unexpected as it is impossible to accurately speculate how far the vehicle can fly, given the remaining energy level.

Despite humans can easily classify colors and segment an image, machines find this task more challenging. As such, image segmentation plays an important role in computer vision applications. To segment an image, based on colors, basic approaches such as color space thresholding (Jain, Kasturi, Schunck, 1995) and nearest neighbor classification (Bruce, Balch, Veloso, 2000) define the segment shapes predicated on the data structures used by the algorithm. Whereas data-driven methods determine the segment shapes using the distribution of the samples to agree with the human perception of colors. There are a multitude of data-driven techniques for color segmentation, such as clustering classification (Sathya & Manavalan, 2011; Bora & Gupta, 2014), artificial neural network (Dong & Xie, 2005; Pujara & Prasad, 2013), region growing segmentation (Tseng & Chang, 1992), and human perception-based texture analysis (Chen, Pappas, Mojsilovic, Rogowitz, 2005). Fuzzy Logic in practical applications, such as remote sensing imagery (Baboo & Thirunavukkarasu, 2014), is a useful tool as an interface between logic and human perception (Freksa, 1994). Bhatia, Srivastava, and Agarwal (2010) used the Takagi-Sugeno fuzzy model to locate faces in an image. They implemented this technique using the HSV (Hue-Saturation-Value) color model. The approach was characterized by its simplicity and inexpensive computation, as well as low false positive rates. Moreno-Cadenas, Gómez-Castañeda, Anzueto-Rios, and Hernández-Gómez (2016) employed the Mamdani type FIS (Fuzzy Inference System) for region segmentation. They applied a weighted average method and used YCbCr color space to produce outputs with higher accuracy.

RGB color space is perfect for machines, but it is not very human-friendly due to being perceptually inconsistent (Ganesan & Rajini, 2014). Another drawback of the RGB is the difficulty to separate the color information from the brightness. Other color models such as the HSV and HSL (Hue-Saturation-Lightness) are more convenient ways for the human to specify colors in software as these color spaces are closer to human perception of colors (Smith, 1978; Saxe & Foulds, 1996; Sobottka & Pitas, 1996). Additionally, the

distribution of a color, in these color spaces, is invariant with the variations of the brightness of illuminance (Chaves-González, Vega-Rodríguez, Gómez-Pulido, Sánchez-Pérez, 2010).

With the classification of a field into a verity of color zones, each zone shall consist of a multitude of points evidencing the corresponding color zone. As the selection of a subset out of a large amount of data is a standard, established approach (Tominaga, 1998), it allows a UAV to scout throughout the field and collect the information of interest, given the retractions of a UAS energy level.

In this paper, following the planning of a near-optimal flight trajectory to cover a field completely, a knowledge-driven approach based on the human perception for colors is employed. This was to digitize and distinguish the field into a variety of the field conditions that various zones of the field evidenced, according to the high-altitude imagery captured. The approach exploited the FIS in the HSV color space to provide a fast, yet fairly accurate, point classification. The classification occurred based on the natural language rules of human intuition to allow simple modification of the classification criteria. To scout, a highly representative, dissimilar subset of points then was selected using the GA (Genetic Algorithm). This provided feasible nondestructive, automatic, and continuous close observation to obtain further information with regard to the field condition. The remainder of this paper is organized as follows. Section 2.1 presents path planning for a field coverage. Section 2.2 introduces a color-based image classification according to the human perception. In section 2.3 the scouting approach is proposed, including sample generation, sample selection, and routing over the selected samples. Section 2.4 provides the experimental fields and tests designed in this research. Section 3 shows the comparison of simulation results, between the computerized sampling and currently in-use sampling, and discussions which lead to the conclusion in Section 4.

1.3 MATERIALS AND METHODS

1.3.1 Coverage Path Planning

1.3.1.1 Path Generation

To plan an effective trajectory for a vehicle to cover a field entirely, predetermined path planning appears vital. An A-B line pattern was used to cover the field with the purpose of having neither overlap nor double coverage. In an A-B line pattern every path is represented by two nodes (Figure 1-1).

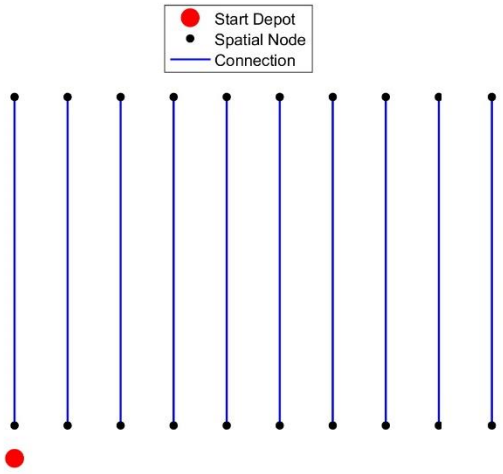

Figure 1-1. A-B line pattern through which each path is represented by two nodes

Agricultural fields are normally decomposed into many working rows. Operations via an aerial vehicle can relax the constraint of travelling along those specific working rows. As such to generate a trajectory for the UAS, numerous parallel paths were created to cover the entire field. The working width of the paths was dependent upon the horizontal field of view ($hFOV$) of the mounted camera on the vehicle, $hFOV = 2 \times (\tan(angle\ of\ veiw)\ /flgithAltitude)$. To ensure the route trajectory for the vehicle was nearly optimal, an exhaustive search algorithm was employed. The vehicle travel direction, θ, to the boundary direction, φ, was changed in 10° intervals. A set of paths, $P = \{p_1, \dots, p_{|P|}\}$, parallel to the longest edge of a field was considered as the initial solution. The objective of this path generation approach was to minimize the working time, $\min(t_{working})$. This happened through minimizing two parameters of working travel and number of turns. The equation for this minimization was as below: (1.1)

$$t_{working}\left(\sum_{p_i \in P} t_{p_i}\right) + |P| \times t_{turn}, i = 1, \dots, |P|$$

where t_{p_i} is the amount of time to travel a path, p_i, t_{turn} is the time a UAV takes to deviate its direction towards the next node. In an autonomous flight, a turn necessitates the vehicle to reduce its velocity to come to a halt, and then to increase velocity to reach to the set velocity, v, i.e., $t_{turn} = \Delta t_d + \Delta t_a$ (Figure 1-2).

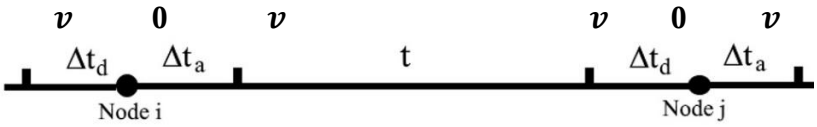

Figure 1-2. The UAV's velocity dynamics to take new direction

1.3.2 Path Planning

Following the generation of the paths, it is essential to route the UAV to fly along the paths. The mathematical representation of the nodes (waypoints) encompassing the field is equivalent to the classical Travelling Salesperson Problem (TSP). In the TSP a salesperson (a vehicle) starts from a designated depot and visits all the customers (nodes) only once. To apply this concept to the field coverage problem, not only are visiting all the customer essential, it is also required to cover the area along every pair of nodes, corresponding to a path. As such, a hard constraint was introduced to ensure that visiting either node of a path forces the vehicle to traverse all the way to the node at the other end of the path. The nodal representation makes the endpoints of paths to be $\{(2q) \cup (2q-1)|q \in \mathbb{N}\}$. Let *G = (N, E)* be an undirected graph where $N = \{n_1, \dots, n_{|N|}\}$ is the set of nodes (waypoints) to be visited by the vehicle, and $E = \{(n_a, n_b): n_a, n_b \in N, a \neq b\}$ is the set of the arcs to connect the node *a* to node *b*, (n_a, n_b). The solution for this problem takes the form of a permutation set of $R_p = \langle n_1, n_2, \dots, n_{|N|} \rangle$. The governing constraints to schedule the paths for the coverage of the field are:

(1) Each pair of nodes, representing a path, are visited consecutively as either node is visited, i.e. $\{(2q_1, 2q_1+1) \vee (2q_1+1, 2q_1), (2q_2, 2q_2+1) \vee (2q_2+1, 2q_2), \dots, (2q_{|P|}, 2q_{|P|}+1) \vee (2q_{|P|}+1, 2q_{|P|})|q \in \mathbb{N}\}$, and

(2) Each node is visited by the vehicle only once, i.e., $|R_p| = |N|$.

For a standard TSP, another constraint applies that requires a route starts and ends at the same location (In the TSP notation, the depot is node 0), i.e., $n_1 = n_{|N|+1} = 0$, and $\{n_2, \dots, n_{|N|}\} \subseteq N \backslash \{0\}$. The coverage problem in this work differs with the standard TSP in this respect. As the initial coverage of the field completes, the vehicle starts scouting the field over a number of representative sample areas, rather than returning to the depot. The return to the deport occurs when the remaining energy disallow further scouting. As

such, the coverage routing is a double-depot variant of the classic TSP, with the second depot as stochastic.

The objective of the path planning was to minimize the amount of time required for the field coverage, $\min(t_{coverage})$.

(1.2)

$$t_{coverage} = \left(\sum_{a \in N} \sum_{b \in N} (t_{ab} + t_{turn}) x_{ab} \right) + t_{take-off}$$

where t_{ab} is travelling time associated with the arc (n_a, n_b), and x_{ab} is a binary variable, which is 1 if the route, R_p, includes a connection between nodes *a* and *b,* and 0 otherwise. To provide a solution for the TSP problem a recursive nearest neighbor (RNN) procedure was adopted (Sturm & Daudet, 2011).

1.3.3 Color-Based Image Segmentation

To classify the image segments into discrete sets of color classes an approach based on human perception was employed. As the HSV color space is more aligned with human perception of colors and avoids the influence of illuminance, the RGB color space of the produced image, using photogrammetry, was converted into the HSV color space. The fuzzy inference system (FIS), then, was utilized in order to classify the image colors presented in the HSV color space, through a fuzzy logic model. In this approach the segments are defined by linguistic terms. The HSV color space is characterized by three values of *Hue, Saturation,* and *Value,* which describe a pure color, the degree of a color dilution with white light, and the brightness of a color, respectively. Each of these parameters were defined as an antecedent variable. Consequently, the conquest variable was defined as the color label.

For the fuzzy logic model utilized in this work 10 fuzzy sets as to Hue variable, $N_{HFS} = \{$Red, Dark Orange, Light Orange, Yellow, Light Green, Dark Green, Aqua, Blue, Dark Purple, and Light Purple$\}$, 5 fuzzy sets for Saturation variable, $N_{SFS} = \{$Gray, Almost Gray, Medium, Almost Clear, and Clear$\}$, and 4 fuzzy sets for Value variables, $N_{VFS} = \{$Dark, Medium Dark, Medium Bright, and Bright$\}$, were defined (Figure 1-3). The Hue variable was normalized in the (0,360) interval, and the Saturation and Value spectrum were considered in the interval of (0,100). Additionally, all the membership functions were defined as triangular functions (Zadeh, 1965). The maximum points of the

membership functions with respect to the Hue variable were determined according to the visual color spectrum.

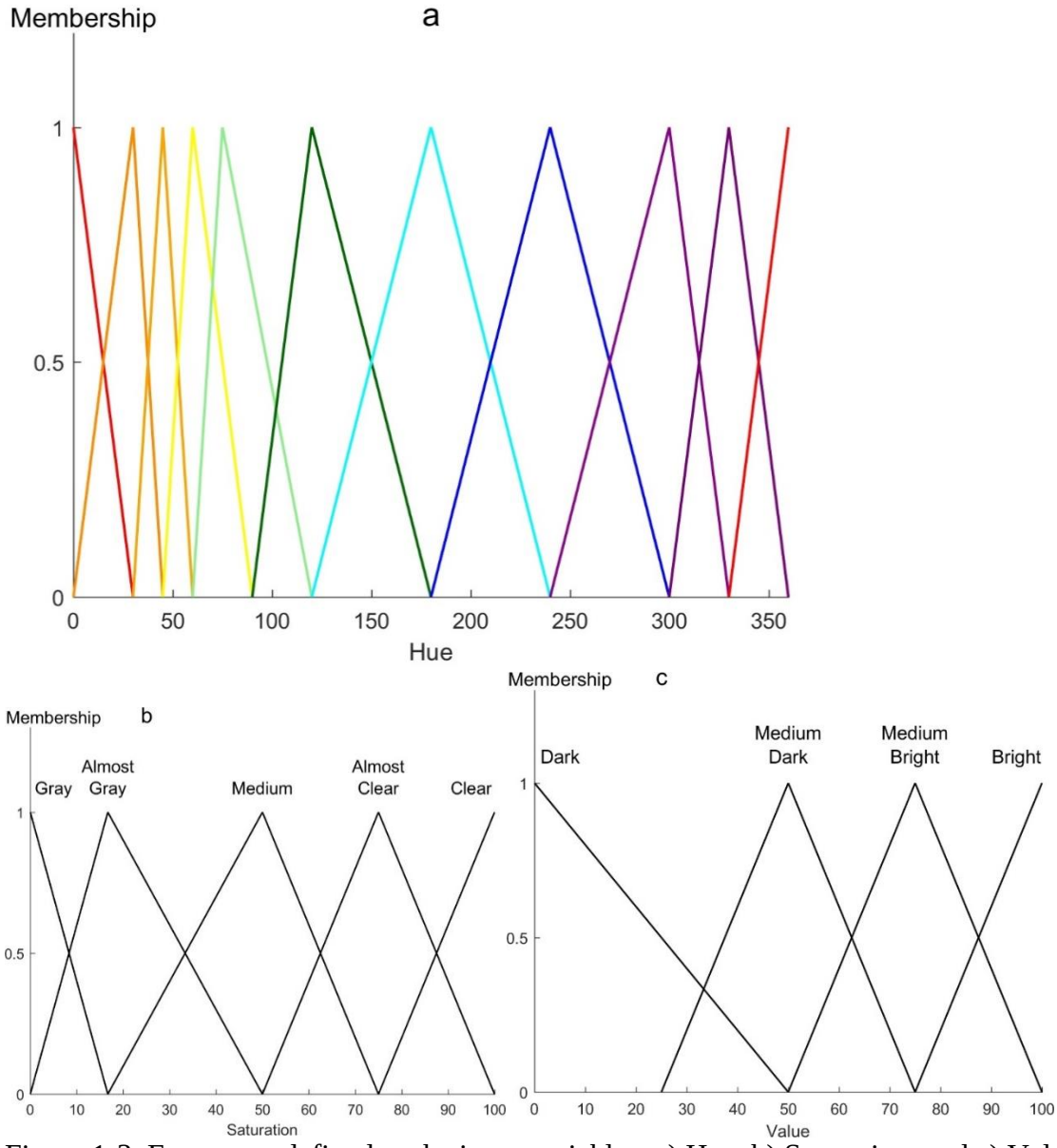

Figure 1-3. Fuzzy sets defined as the input variables, a) Hue, b) Saturation, and c) Value

To have the field segmentation according to human perception, fuzzy rules were defined based on human observations. For instance, the rule "*Yellow* ∧ *Almost Clear* ∧ *Medium Dark* ⟼ *Olive Green*" was determined through manually classifying the color generated by the triple of the HSV. The Hue, Saturation, and Value values are associated with the value of maximum point for the membership function of the *Yellow, Almost Clear, and Medium Dark* fuzzy sets, respectively, i.e., $H = 60$, $S = 75$, and $V = 50$.

Finally, for the determination of crisp discrete values as the consequent part, the reasoning procedure took place according to a zero-order Takagi-Sugeno (Takagi & Sugeno, 1983; Takagi & Sugeno, 1985). The crisp discrete values consisted 13 distinct colors of *Dark Orange, Gold, Yellow, Lime, Green, Dark Cyan, Blue, Pink, Magenta, Red, Black, Grey,* and *White*. In aggregate, 200 fuzzy rules, $|N_{FR}| = N_{HFS}| \times |N_{SFS}| \times |N_{VFS}|$, were defined.

1.3.4 Scouting Procedure

1.3.4.1 Sample Generation

Classifying the entire field according to the fuzzy logic system resulted in a spectrum of colors. In this work the primarily focus was places upon four specific colors of *green, lime, yellow,* and *red* indicating healthy and grown zone, healthy and undergrown zone, water stressed zone, and drown out zone (VanderLeest, Bergman, Darr, Murphy, 2016). Other colors associated with the non-zone of interest (ZOI) were disregarded. The luminance of point, then, was computed to determine their value. The luminance was achieved as the average of the largest and smallest *R, G,* and *B* color channels, i.e., $L = \frac{1}{2}(M + m)$ where *M* is *max(R,G,B)* and *m* is *min(R,G,B).* The luminance was normalized to the interval of (0,100). This generated a normal distribution with the mean corresponding to the highest value of the associated color (Figure 1-4).

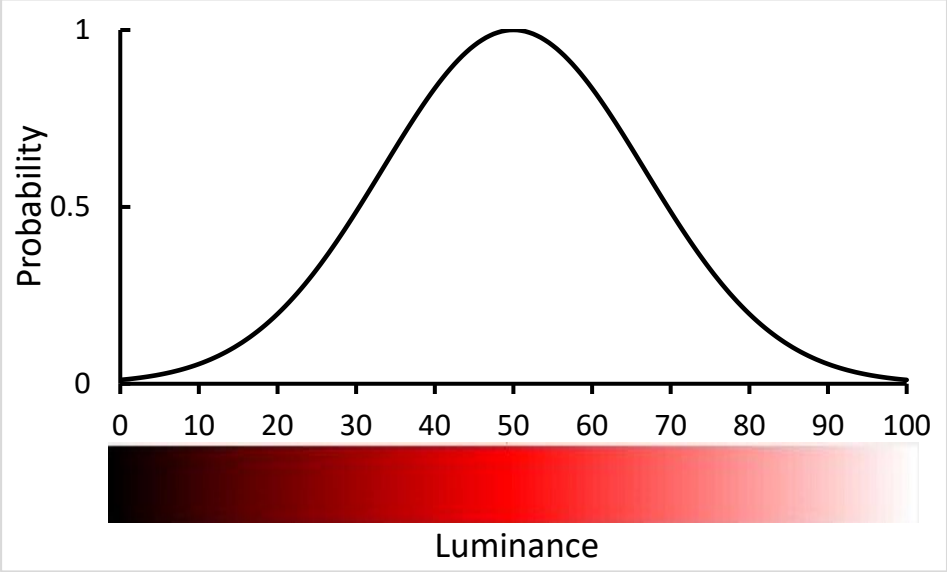

Figure 1-4. Normal distribution of the luminance of red index

Furthermore, to improve the probability that a point is a true representative of a specific ZOI, the area of each point was expanded. As such every block of points, $m \times m$ points, was indexed as the index of the dominant feature. This reduced the number of points by a factor of m^2, i.e., $S_{block} = S_{all}/m^2$. Therefore, the luminance for each block point can be represented as:

$$L = \begin{bmatrix} l_{11} & l_{12} & \cdots & l_{1J/m} \\ l_{21} & l_{22} & \cdots & l_{2,J/m} \\ \vdots & \vdots & \cdots & \vdots \\ l_{I/m,1} & l_{I/m,2} & \cdots & l_{I/m,J/m}* \end{bmatrix}$$

* I indicates the max number of the pixels along the y axis and J is the max number of the pixels in the x axis

For better indexing of each block, the most frequent color index constituting a block was chosen as the new index of the block. For blocks consisting of an equal number of color indices as the highest frequent indices, decision was made based on the previous block index to maintain consistent index; subsequent block index was taken into consideration, if it would be the case the previous block index was an index different than the current two dominant indices. In the event of inconsistency of the previous and subsequent block index with the current block, the current block was indexed according to the index of the first highest frequent color. The value of a block sample was determined based on the average value of the comprising samples. In this work, only blocks with the consistent index for all their comprising pixels were considered valid. Additionally, to squeeze the number of samples into the more representative samples of their corresponding feature, thresholding was applied on the luminance of the samples (Figure 1-5).

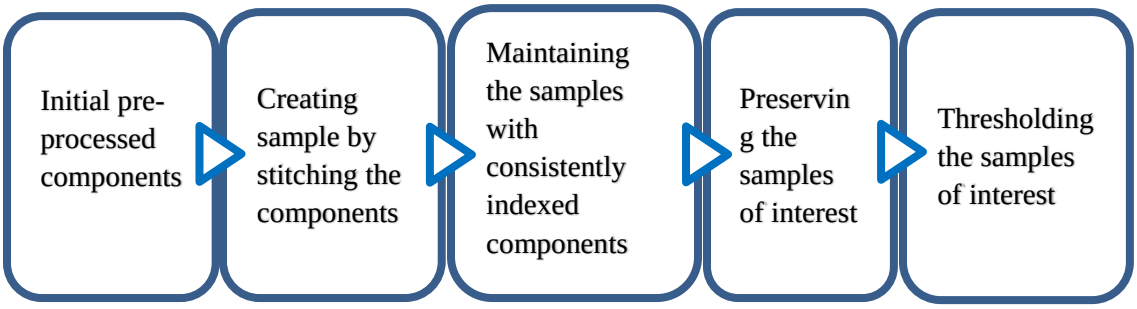

Figure 1-5. Steps taken to generate samples for scouting

1.3.5 Sample Selection

In order to collect sufficient information of a field a number of considerations are essential in the process of the sampling. First is to have highly representative samples from possibly all segments with different features. Second is the number of distributed samples through which more robust conclusion would be drawn. Additionally, efficient routing is another parameter that allows to visit the samples in an order to consume less energy.

1.3.5.1 Conventional Approach

To manually select samples from various regions of the field, two approaches were taken into consideration: grid sampling, human expert sampling. The grid sampling considered a fixed number of samples located in the intersection of each grid. In this method, the representative samples were selected based on their geographical location and their associations to different color zones was initially unknown. The vehicle started visiting the nearest sample to the last node, flown over while the field coverage, and followed a pre-determined route to visit all the samples associated with the grid intersection. When it would be the case that the battery was only sufficient to travel to the start node, the vehicle stopped sampling and traveled straightly to the depot. The human expert sampling took place in a drastically more promising, efficient manner. In this method, an agriculture engineer, who was experienced in agricultural operations, was asked to select meaningful samples. It was assumed, upon the field coverage, the vehicle communicates with a human expert to send the data associated with the covered area and to receive the position information of selected samples.

A number of considerations were taken into account as to the human expert method. Unlike the grid sampling, the sampling was conducted consistently for different color zones in terms of quantity. The samples were selected given the location of last node, following the field coverage, and start depot corresponding to each scenario. This allowed the vehicle to visit more samples due to more efficient energy consumption. Additionally, the trajectory through which samples were visited was thoughtfully planned to contribute to less energy consumption.

The human expert method of sampling also took place according to the importance of the color zones: equal-weight zones and non-equal-weight zones. For the

equal-weight zones, all samples assumed to have the same weight, and as such the equal number of samples associated with each color zone was selected. Whereas with regard to the non-equal-weight zones, each color zone was assumed carrying different weight, dependent upon the significance associated with its zone. This happened via taking various number of samples corresponding to each color zone.

1.3.5.2 Computational Approach

The computation-based approach necessitated a two-fold procedure to be effective: representative sample selection, and efficient routing of the selected samples.

Sample Selection

Visiting all or many of the samples constituting the entire field is a time consuming task and results in redundant information. Given the battery life restriction, however, only a small fraction of the samples can be visited by the vehicle. As such, selecting a subset of the samples appears a viable solution. Let the subset of samples be a set of samples that creates a population S, $S = \langle s_1, s_2, \dots, s_{|S|} \rangle$ where each s represents a selected sample. The governing constraints for the number of selected samples are:

1) The routing of the samples starts from the last node flown over in the field coverage, $n_{|N|}$, and ends to the depot, n_1, i.e., $R_s = \langle n_{|N|}, s_1, s_2, \dots, s_{|S|}, n_1 \rangle$.
2) The total time to visit the entire subset of samples by the vehicle, and return to the depot must be less than or equal the remaining battery life time of the vehicle, i.e.,

$$t_{scouting} = \left\{ \sum_{a \in S} \sum_{b \in S} (t_{ab} + t_{turn}) x_{ab} \right\} + t_{landing} < t_{remaining}$$

The next step was the creation of a fitness function that appropriately captures the optimization criteria of the problem. The primary parameter with a resulting efficient scouting is the total scouting luminance (TSL),

(1.3)

$$TSL = \sum_{i \in S_{block}} \sum_{j \in S_{block}} w_{ij} l_{ij} x_{ij}, i = 1, 2, \dots, I/m \text{ and } j = 1, 2, \dots, J/m$$

where x_{ij} is a binary variable, which is 1 if the selected samples, *S*, includes a the sample in the i^{th} row and j^{th} column, (i, j), of the S_{block}, and 0 otherwise. w_{ij} is the weight assigned to the sample, (i, j). Hence the goal is to maximization of the this parameter, $\max(TSL)$.

The above fitness function increases the probability of the representativeness of selected samples. Another important parameter is to collect knowledge with regard to the all ZOIs. This necessitates improving the dissimilarity of the selected samples, i.e.,

(1.4)

$$sample_{min} = min_{k|k\in index} \sum_{i\in S}\sum_{j\in S} x_{ijk}\,, index = \{e, g, u, s\}$$

The added variable, *k*, allows to calculate the number of samples representing each color zone individually.

Although having more samples provides more information as to the status of a field, evaluating each solution simply based on the number of samples is not suitable. There is a high likelihood to fail in the collection of knowledge with respect to one or more color zones. As such, a fitness function based on double objectives optimization was defined.

(1.5)

$$\max\big(z \times TSL - (1-z)(sample_{max} - sample_{min})0.01M - (M - xM)\big)\,, z|0 \le z \le 1$$

where *z* represents the focus is placed on the optimization of the TSL versus sample diversity (SD). Utilizing a weighting function enables adjusting the focus of the optimization for producers who may also want a balance between obtaining highly representative samples and equal amount of knowledge from the various ZOIs. In this project, the primary focus was on the selection of highly representative samples. In initial testing, a weighting value of 0.60 was found to provide sufficient optimization in sample selecting from all ZOIs while still selecting samples that maximized the TSL.

Solution Method

To provide solutions for the mathematical representation developed for the sample selection, a metaheuristic procedure based on Genetic Algorithm (GA) was employed. As with other meta-heuristics, like neural networks or tabu search, there are many implementations for the GA. This technique is an adaptive heuristic, population based, and stochastic search procedure to find approximate or near optimal solutions for optimization problems (Goldberg, 1989). Each chromosome in the population set is a possible solution for the problem. The algorithm creates a series of populations in each successive iteration using a selection mechanism, based on the fitness function. The GA exploits the intelligent random search within a solution space.

The GA utilized in this study used two primary operators as search mechanism: cross-over and mutation. Each chromosome was encoded into integers, representing the luminance of a number of samples. The number of comprising gens (selected samples) varied for each chromosome, dependent upon the energy level required to fly over the samples. To implement the algorithm, the best solution generated through the conventional approaches was taken into consideration as the initial population. Hence, the main focus was placed upon the operators, so the number of population created through the cross-over was 5% of the number of the block samples, i.e., $|P_{cross-over}| = 0.05 \times |S_{block}|$. Population created using mutation was 20% as many number as the cross-over population, i.e., $|P_{mutation}| = 0.2 \times |P_{cross-over}|$.

The GA was implemented in MATLAB. First, the algorithm determined all populations based on cross-over and mutation operators. Using this array of possible solutions, the algorithm then applied selection mechanism, based on the fitness value, to improve the prior individual solution. The best permissible gene string was selected unless the optimization criterion was not met, i.e., the fitness value was less than the global (prior) solution. Finally, a new solution was generated. This procedure was repeated with continuously improving solutions until 100 iterations had passed with no improvement. At this point, the algorithm halted and provided its best solution as the optimized selected samples. In preliminary experiments, the total number of iterations was usually between 300 and 400.

Routing Over Selected Samples

Upon the determination of samples to visit, it is vital to fly over the samples following a short, optimal trajectory. As with the path planning for the field coverage, visiting the selected samples can be viewed equivalent to the double-depot TSP— the last node flown over in the field coverage, $n_{|N|}$, and ends to the depot, n_1. As to the constraints, however, the constraint (1) shall be relaxed as the primary goal is to merely fly over the sample areas. The objective of this TSP problem was also to minimize the time to visit the selected samples and return to the depot, min($t_{scouting}$). As such the fitness function was defined the same as the objective function.

The GA was also employed to provide solutions as to routing the UAV over the selected samples. Unlike the GA procedure used for the sample selection, many

chromosomes (50 gene strings) were created as initial population. The cross-over and mutation operators, then, were applied, $|P_{cross-over}| = 0.8 \times |P_{initial}|$ and $|P_{mutation}| = 0.2 \times |P_{cross-over}|$, respectively. This procedure was repeated with continuously improving solutions until 50 iterations had passed with no improvement.

This procedure to create solutions as to routing over the selected samples was embedded into the GA procedure of the sample selection. This allowed shortening the travel time and creating the opportunity to visit several more samples, in each iteration.

1.3.6 Test Conditions

The objectives of this work were pursued based on computer simulations. To that end, the developed procedure was tested on two real-world fields with different characteristics in terms of shape, size, and complexity. The first field was a non-convex shaped, 86-hectar field located at the Kossuth, Iowa [43.265,-94.016], on which soybean had been planted (Figure 1-6 a). The second field was a convex shaped, 133-hectar field at the Bremer, Iowa [42.697,-92.502], on which corn had been planted (Figure 1-6 b).

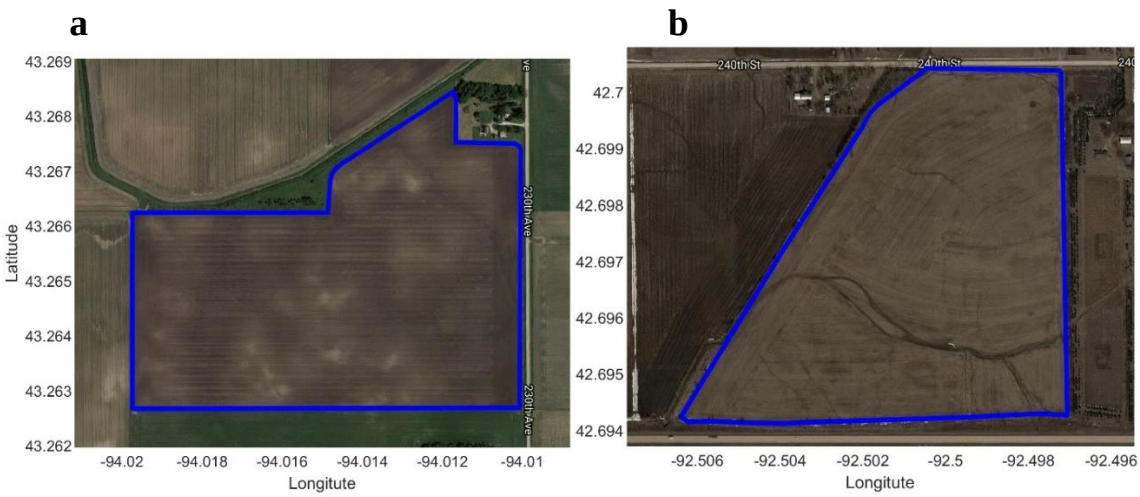

Figure 1-6. Test field located at a) Kossuth, b) Bremer, Iowa

To cover each field, three variable parameters were defined. 1) the vehicle velocity (traveling at low velocity, 10 m/s, or high velocity, 15 m/s), associated to the kinematics of a UAS; 2), the starting location (three different locations where were more appropriate to initiate the mission), related to the geographical properties of the fields; and 3) the weight assigned to each color zone (twice as much as other color zones for that

of higher importance), associated with decisions as to the field condition. As such, 24 test scenarios were designed for each test field to assess all the combinations (Table 1-1).

Table 1-1. Test scenarios designed for each field with respect to the vehicle velocity, the starting location of the mission, and the weight of each color zone

Scenario Abbreviation*	Vehicle Velocity (m)**	Starting Location State	Weight of Color Zone***			
			Healthy and Grown	Healthy and Undergrown	Water Stressed	Drown-Out
V10S1We	10	1	1	1	1	1
V10S1Wg	10	1	2	1	1	1
V10S1Wu	10	1	1	2	1	1
V10S1Ws	10	1	1	1	2	1
V10S2We	10	2	1	1	1	1
V10S2Wg	10	2	2	1	1	1
V10S2Wu	10	2	1	2	1	1
V10S2Ws	10	2	1	1	2	1
V10S3We	10	3	1	1	1	1
V10S3Wg	10	3	2	1	1	1
V10S3Wu	10	3	1	2	1	1
V10S3Ws	10	3	1	1	2	1
V15S1We	15	1	1	1	1	1
V15S1Wg	15	1	2	1	1	1
V15S1Wu	15	1	1	2	1	1
V15S1Ws	15	1	1	1	2	1
V15S2We	15	2	1	1	1	1
V15S2Wg	15	2	2	1	1	1
V15S2Wu	15	2	1	2	1	1
V15S2Ws	15	2	1	1	2	1
V15S3We	15	3	1	1	1	1
V15S3Wg	15	3	2	1	1	1
V15S3Wu	15	3	1	2	1	1
V15S3Ws	15	3	1	1	2	1

* V represents Velocity (m/s); S represents Start/Stop location; and W indicates which color zone is weighted as the highest (e indicates equal weight for all samples, and g, u, and s are associated with the healthy and grown, healthy and undergrown, and water stressed zones, respectively.
** The higher velocity of 15 m/s is the maximum velocity the DJI Ground Station Pro app allows to fly.
*** This was conducted with respect to the healthy and grown zone, healthy and undergrown zone, and water stressed zone

In order to classify various zones of each field the NDVI was employed. The NDVI is an index to monitor crop photosynthetic activity and health. This index can be calculated through the Near-Infrared (NIR) and Red imageries, $NDVI = NIR - Red/NIR + Red$. The NDVI images provided for the both fields in this work were derived by the Iowa Soybean Association. The Figure 1-7 represents colors in the NDVI images, while the field was grown for corn.

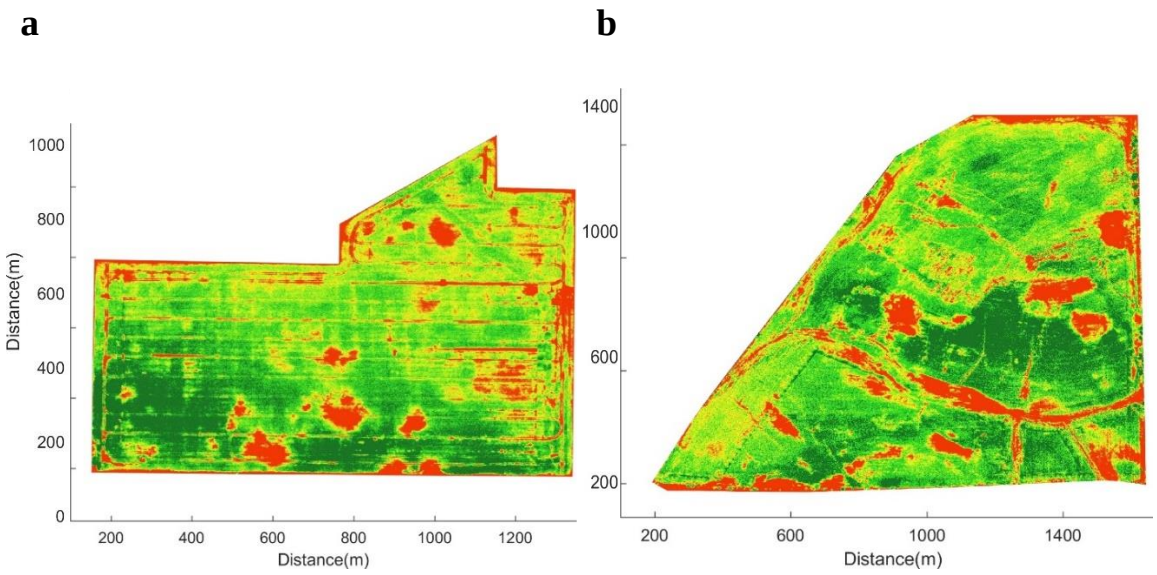

Figure 1-7. NDVI image created for the a) Kossuth field and b) Bremer field

As to the grid approach, the Kossuth field constituted 10 intersections, with dividing up the entire field into 17 sub-regions. The samples located at the intersections included 2, 5, and 3 representatives of healthy and undergrown, water stressed, and drown out zones. This approach did not consist of a sample representing healthy and grown zones, respectively. The Bremer field also comprised of 9 intersections by its division into 17 sub-sections. The approach relied on 1, 2, 4, and 2 points representing the healthy and grown, healthy and undergrown, water stressed, and drown out zones, respectively. Whereas, the human expert selected consistently 3 samples associated with each color zone and doubled it for the color zones with higher weight.

The UAV considered in this study as the test platform was the 2016 Mavic Pro (DJI, China) which uses lens with the FOV of 78.8° 28 mm (DJI, 2017). Therefore, as the highest flight altitude set by the FAA is 400 feet, the $hFOV$ was calculated to be 200 m. To implement the field tests, 30% of the battery life was maintained unused as return home energy (RHE). This level of RHE is set as default by DJI to allow the vehicle to return home and land in case of in-operation contingencies such as loss of control signals. The RHE level for the scenarios as to flying at slower rate on the Bremer field, however, was set at 15%, as the vehicle energy was consumed primarily for the initial coverage.

1.4 RESULTS

1.4.1 Coverage Path Planning

The coverage time of the Kossuth field and Bremer field are demonstrated in Figure 1-8 for 6 different scenarios: vehicles' velocity of 10 m/s and 15 m/s at three different starting locations. The direction change of the parallel paths with respect to the field boundary reduced the number of paths, and accordingly the numbers of nodes were minimized to 10 and 14 nodes for the Kossuth and Bremer fields, respectively. The Kossuth field coverage was completed with the average consumption of 75% (883 s) and 57% (666 s), of the permissible UAV's battery life, while flying at low velocity, 10 m/s, and high velocity, 15 m/s, respectively. Even though, the total area of the Bremer field was 55% larger than the Kossuth field, the Bremer field coverage time was not that much longer (30% longer at both low and high velocities). This was due to the more regular shape of the Bremer field that enabled reducing the non-working travel time and the number of nodes. The position 2 of the starting location allowed completing the field in less time, approximately 3%, than the other positions, in both the Kossuth and Bremer fields (Figure 1-9). This stemmed from the minimization of non-working travel and overlap-area, due to the proximity of the vehicle to the first path created for the field coverage. The reduction was also for the efficient generation of nodes and the routing to cover the field.

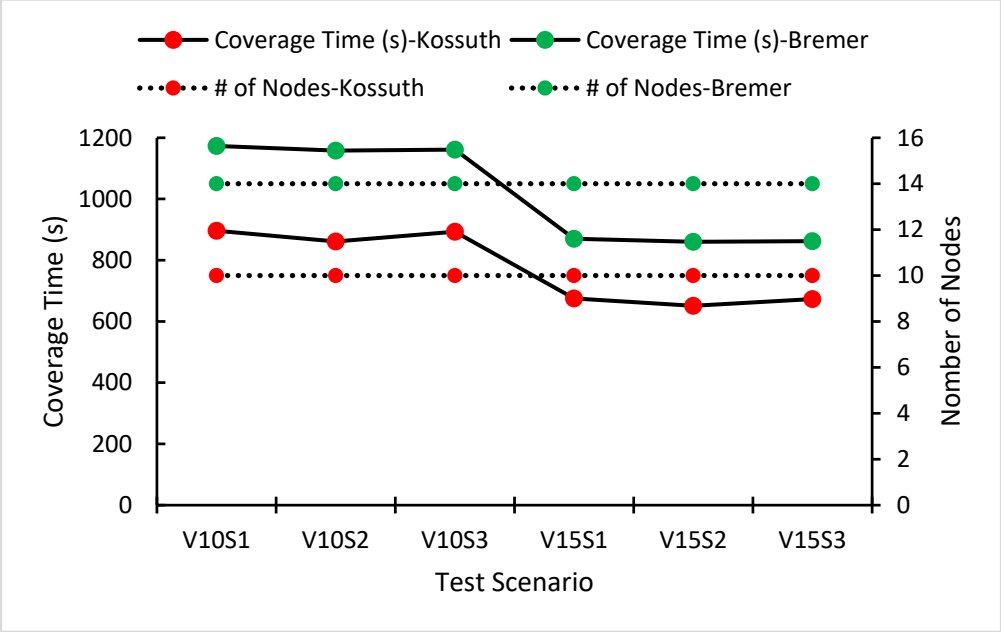

Figure 1-8. Coverage time of the fields under various circumstances

With the high flight velocity, the coverage time improved nearly 25% for both the Kossuth field and Bremer field. As with the field area ratio, the improvement was not consistent with the flight velocity ratio which was 50% faster than the low velocity. This was not unexpected, as the trajectory planned to cover the field generated nodes, regardless of the vehicle velocity, which were associated with the vehicle turns. These turns took 53 s for the Kossuth field and 74 s for the Bremer field (5.3 s per turn), to complete. As such, the time reduction, due to the increase in velocity, occurred solely on the portion of the time spent for forward travelling. The number of nodes depended upon a multitude of parameters such as the field area and the complexity of the field's shape. It also depended on the flight altitude which determined the $hFOV$ that was the same for to cover both fields in this work, $hFOV = 200\ m\ @\ 400\ feet$ flight altitude.

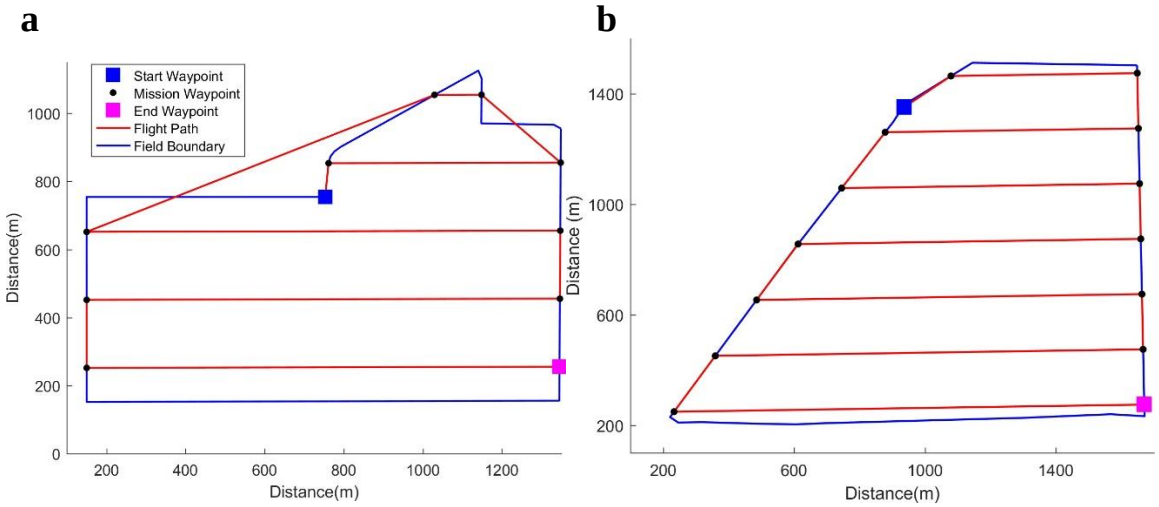

Figure 1-9. Route generated for the entire coverage of a) Kossuth field and b) Bremer field when the mission starts at the state 2 of starting locations

1.4.2 Segmentation

1.4.2.1 Fuzzy Logic-Based Color Classification

The color-based classification of the Kossuth and Bremer fields, through the fuzzy logic model, are illustrated in Figure 1-10. Both fields were classified in 6 distinct color zones: *Dark Orange, Gold, Yellow, Lime, Green,* and *Red.* As displayed the color zones derived using the FIS correlate accurately with the NDVI mapping. Throughout the fields *Yellow, Lime, Green,* and *Red* color zones were respectively associated with

healthy and grown, healthy and undergrown, water stressed, and drown out zones. These zones made up 86% of the Kossuth field and 89% of the Bremer field.

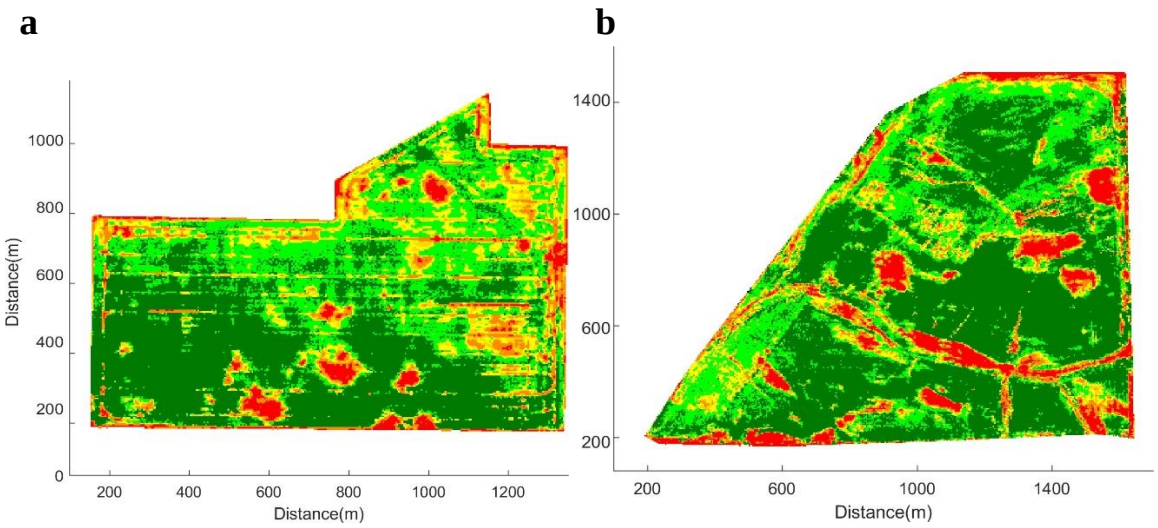

Figure 1-10. Color-based segmentation using the fuzzy inference system for the a) Kossuth field and b) Bremer field

The computational time to perform the FIS was in an order of magnitude of a few seconds, on an Intel i7 processor. This low computation complexity was stemming from the constant number of the reasoning rules in the model, and the fact that the classification of each pixel was conducted with the same constant complexity. As such this knowledge-driven model can be implemented on mobile autonomous vehicle for real-time application.

1.4.3 Scouting

1.4.3.1 Sample Generation

Table 1-2 represents the number of possible samples generated for the Kossuth and Bremer fields. The area of each block point, due to stitching the components, was 16 m (n = 4). This reduced the number of points by a factor of 16. The elimination of the points with inconsistent indices in their comprising components substantially decreased the number of points, by 65% and 87.6% for the Kossuth and Bremer fields, respectively. Following the determination of the valid samples, the samples corresponding to the *Dark Orange* and *Gold* color zone were removed. The last step of the generation of representative points maintained 32.5% and 22% of the total samples, for the Kossuth and Bremer fields, respectively (Table 1-2).

Table 1-2. Number of generated samples

Test Fields	Point Area (m^2)	# of Total Points	# of Valid Points	# of Valid & of Interest Points	# of Points with High Luminance*
Kossuth Field	16	53350	18675	17355	17354
Bremer Field	16	86221	19302	19003	19003

* High luminance samples are determined after truncating the spots through thresholding.

The distribution of the valid representative samples for the color zones of interest is displayed in Figure 1-11. As shown, in both fields the healthy and grown points outnumbered the other types of points, approximately 75% of the entire samples. Whereas the respective percentage of the healthy and undergrown, water stressed, and drown out samples were 12.6%, 7.5%, and 6.2% for the Kossuth field and 2.3%, 2.5% and 17.9% for the Bremer field.

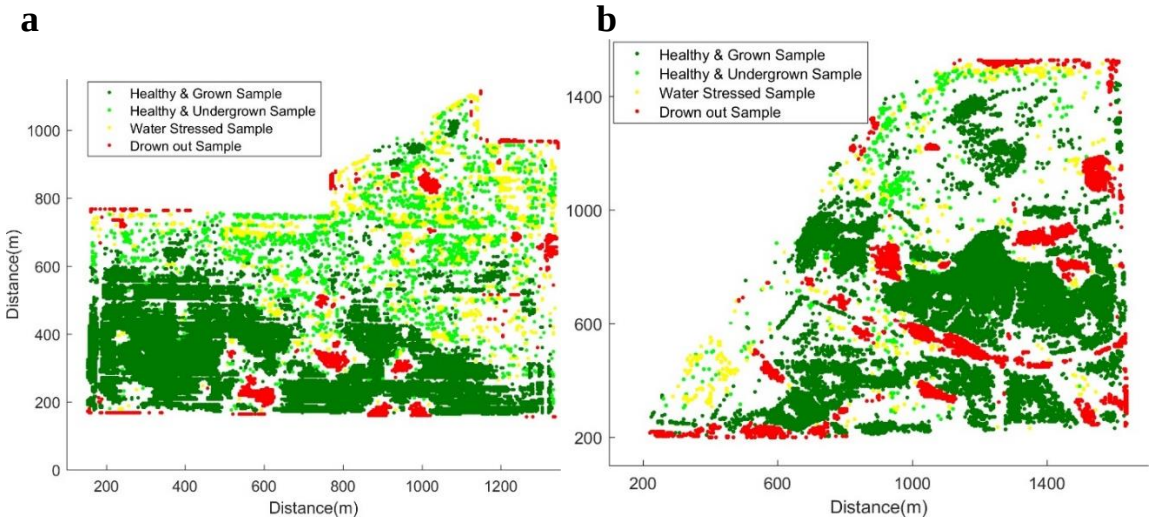

Figure 1-11. Samples considered as valid representatives of each color zone a) Kossuth field and b) Bremer field

1.4.4 Sample Selection

1.4.4.1 Farmer Approaches

Tables 1-3 and 1-4 represent the results of the two approaches that were employed as current farmers methods for sampling. The human expert sampling consistently outperformed the grid sampling method in terms of the number of samples visited, given the same amount of flight time remained following the field coverage. This increase occurred, regardless of the type of the samples, by up to 120% for the Kossuth field and

55% for the Bremer field. However, in both approaches the vehicle used its energy up to a nearly equal level that the remaining energy was insufficient to travel over the next samples. The highest remaining energy in Kossuth field was 42s, following the grid sampling and 32s, following the human expert sampling, in the event of not visiting the entire samples. Whereas in the Bremer field, the remaining energy increased to be 52s and 51s for the grid and human expert samplings. This was expected as the Bremer field was nearly 55% larger than the Kossuth field, and as such travelling over the next sample area was necessitating more energy.

Unlike following the grid sampling, the number of samples visited in the human expert sampling varied, for the scenarios that the entire samples were not visited, dependent on which color zone had higher fitness weight. This arose from the fact that the human expert paid a rigorous attention to the selection of the samples highly representative of each ZOI, while the grid sampling method was invariant to the color zone weights. The human expert sampling also resulted in visiting higher representative points corresponding to the ZOIs, in nearly all scenarios, by up to 8%.

Table 1-3. Scouting though farmer approaches for Kossuth field

Test Scenarios	RHE (%)	Grid Sampling					Human Expert Sampling				
		# of Samples	ASP	TSL	SD (%)	Remaining Energy (s)	# of Samples	ASP	TSL	SD (%)	Remaining Energy (s)
V10S1We	30	7	0.88	6.13	75	4	8	0.95	7.63	100	14
V10S1Wg	30	7	0.88	6.13	75	4	7	0.95	6.63	75	28
V10S1Wu	30	7	0.88	6.13	75	4	7	0.95	6.65	100	19
V10S1Ws	30	7	0.88	6.13	75	4	8	0.95	7.63	100	13
V10S2We	30	8	0.89	7.12	75	28	12	0.96	11.54	100	1
V10S2Wg	30	8	0.89	7.12	75	28	11	0.95	10.44	100	25
V10S2Wu	30	8	0.89	7.12	75	28	11	0.97	10.69	100	32
V10S2Ws	30	8	0.89	7.12	75	28	12	0.97	11.62	100	15
V10S3We	30	5	0.97	4.84	75	42	9	0.96	8.64	100	21
V10S3Wg	30	5	0.97	4.84	75	42	9	0.95	8.52	100	23
V10S3Wu	30	5	0.97	4.84	75	42	10	0.96	9.64	100	1
V10S3Ws	30	5	0.97	4.84	75	42	11	0.97	10.62	100	11
V15S1We	30	10	0.91	9.10	75	252	12	0.97	11.60	100	260
V15S1Wg	30	10	0.91	9.10	75	252	15	0.96	14.35	100	198
V15S1Wu	30	10	0.91	9.10	75	252	15	0.97	14.58	100	199
V15S1Ws	30	10	0.91	9.10	75	252	15	0.97	14.51	100	220
V15S2We	30	10	0.91	9.10	75	288	12	0.96	11.54	100	293
V15S2Wg	30	10	0.91	9.10	75	288	15	0.94	14.13	100	253
V15S2Wu	30	10	0.91	9.10	75	288	15	0.97	14.53	100	258
V15S2Ws	30	10	0.91	9.10	75	288	15	0.96	14.46	100	260
V15S3We	30	10	0.91	9.10	75	246	12	0.95	11.45	100	267
V15S3Wg	30	10	0.91	9.10	75	246	15	0.95	14.22	100	221
V15S3Wu	30	10	0.91	9.10	75	246	15	0.96	14.44	100	225
V15S3Ws	30	10	0.91	9.10	75	246	15	0.96	14.41	100	243

* V represents Velocity (m/s); S represents Start/Stop location; and W indicates which color zone is weighted as the highest (e indicates equal weight for all samples, and g, u, and s are associated with the healthy and grown, healthy and undergrown, and water stressed zones, respectively.

Table 1-4. Scouting though farmer approaches for Bremer field

Test Scenarios	RHE (%)	Grid Sampling					Human Expert Sampling				
		# of Samples	ASP	TSL	SD (%)	Remaining Energy (s)	# of Samples	ASP	TSL	SD (%)	Remaining Energy (s)
V10S1We	15	3	0.91	2.72	75	22	4	0.96	3.82	100	12
V10S1Wg	15	3	0.91	2.72	75	22	4	0.96	3.82	100	12
V10S1Wu	15	3	0.91	2.72	75	22	4	0.96	3.82	100	7
V10S1Ws	15	3	0.91	2.72	75	22	4	0.96	3.82	100	2
V10S2We	15	5	0.89	4.45	75	12	6	0.95	5.69	100	16
V10S2Wg	15	5	0.89	4.45	75	12	5	0.94	4.72	100	21
V10S2Wu	15	5	0.89	4.45	75	12	7	0.96	6.69	100	8
V10S2Ws	15	5	0.89	4.45	75	12	5	0.96	4.82	75	6
V10S3We	15	4	0.90	3.60	50	21	5	0.96	4.81	75	17
V10S3Wg	15	4	0.90	3.60	50	21	5	0.96	4.81	75	17
V10S3Wu	15	4	0.90	3.60	50	21	5	0.97	4.85	75	23
V10S3Ws	15	4	0.90	3.60	50	21	5	0.97	4.83	75	9
V15S1We	30	9	0.92	8.27	100	30	12	0.95	11.44	100	34
V15S1Wg	30	9	0.92	8.27	100	30	12	0.93	11.20	100	6
V15S1Wu	30	9	0.92	8.27	100	30	12	0.96	11.55	100	12
V15S1Ws	30	9	0.92	8.27	100	30	12	0.96	11.56	100	21
V15S2We	30	9	0.92	8.27	100	52	12	0.96	11.48	100	57
V15S2Wg	30	9	0.92	8.27	100	52	13	0.95	12.30	100	21
V15S2Wu	30	9	0.92	8.27	100	52	12	0.97	11.59	100	51
V15S2Ws	30	9	0.92	8.27	100	52	11	0.96	10.58	100	46
V15S3We	30	9	0.92	8.27	100	31	12	0.95	11.44	100	45
V15S3Wg	30	9	0.92	8.27	100	31	14	0.94	13.11	100	3
V15S3Wu	30	9	0.92	8.27	100	31	14	0.96	13.44	100	1
V15S3Ws	30	9	0.92	8.27	100	31	13	0.96	12.49	100	12

* V represents Velocity (m/s); S represents Start/Stop location; and W indicates which color zone is weighted as the highest (e indicates equal weight for all samples, and g, u, and s are associated with the healthy and grown, healthy and undergrown, and water stressed zones, respectively.

Furthermore, the TSL achieved through the human sampling and routing consistently increased compared to the grid routing. The average improvements were 53% and 38%, with standard deviations of 26% and 12%, for the Kossuth and Bremer fields, respectively (Figure 1-12 and Figure 1-13). The improvement maintained a constant pattern in the event all the samples were visited, as for the Kossuth field with the vehicle velocity at 15 m/s. Whereas in case of the uncompleted visits the magnitude of the improvement varied dependent solely upon how the human expert decided on samples' locations and routing. Additionally, the improvement of the TSL is directly and linearly impacted by the increase in the samples numbers. The marginal increase in the TSL improvements, compared to the improvements of the samples numbers, came from the betterment of the samples (being more representative of their corresponding zones) selected by the human picker (Figure 1-12 and Figure 1-13).

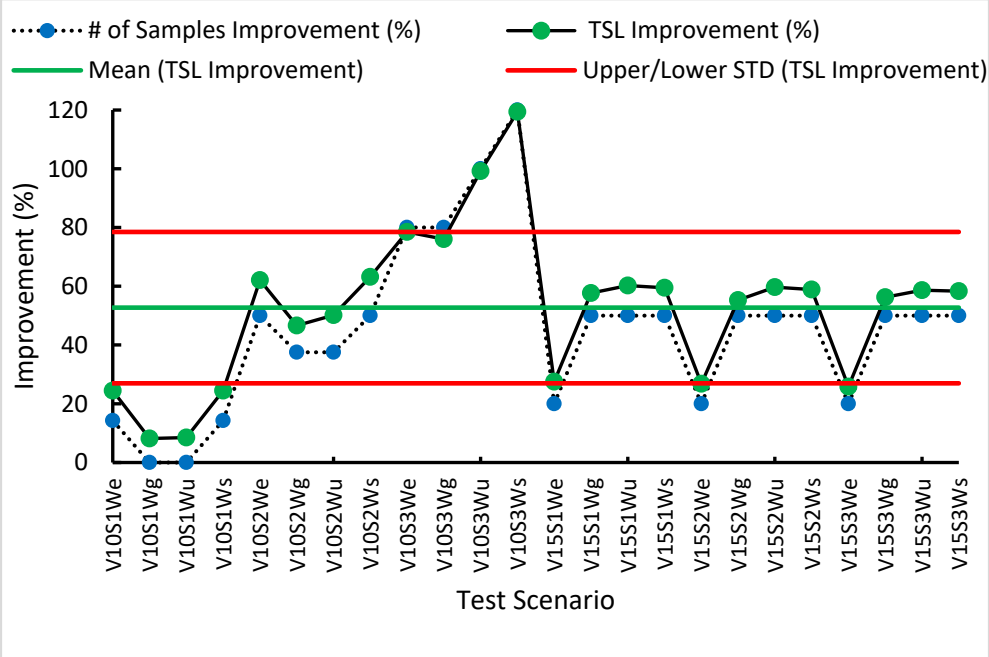

Figure 1-12. The percentage of TSL improvement through the Human Expert Routing compared to the Grid Routing approach for Kossuth field

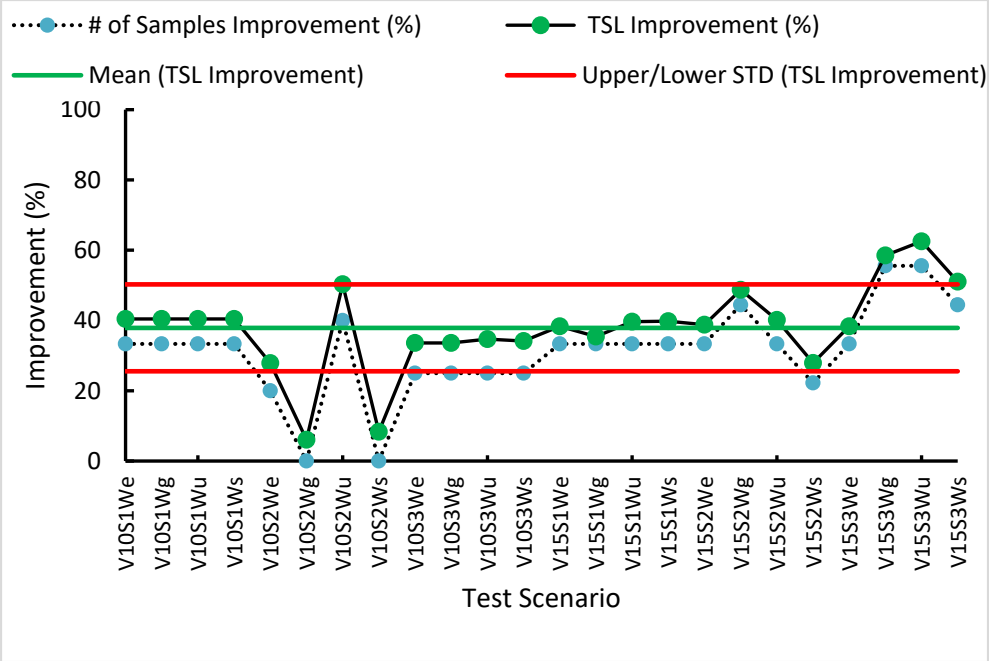

Figure 1-13. The percentage of TSL improved through Human Expert Routing compared to Grid Routing approach for Bremer field

A representative example route of the grid and human expert approaches have been displayed in Figure 1-14 and Figure 1-15. As to the Kossuth field, the route represents a scenario in which the UAV began the mission at the position 2 as the start location, flying at 10 m/s, and the fitness weight considered for the water stressed zone was twice as much as other zones (V10S2Ws). Following the grid sampling, the vehicle visited the first eight intersections and returned to the depot, as it lacked energy to visit the next samples. The intersections visited by the vehicle consisted of the healthy & grown, healthy & undergrown, and water stressed zones, but not the drown out zone. As such the sample diversity accounted for 75%. Whereas, following the human selected samples encompassed all four zones of interest (a SD of 100%). For this instance, the high emphasis was put on the water stressed zones. As such this zone accounted for 5 samples out of 12 visited samples.

The route with respect to the Bremer field (Figure 1-15) demonstrates a scenario in which vehicle traveled at 15 m/s (V15S3Wu). The high velocity enabled the vehicle to visit all the intersections, then return to the depot, with some energy remained. Following the human determined samples and route, however, the vehicle was unable to visit the last sample due to the insufficient power. As the last sample lay on the flight path to the

depot, a quick shot at lower altitude was collected without letting the vehicle decelerate and focus on the sample area. The higher fitness weight was placed on the healthy & undergrown zones, so the number of corresponding samples consisted of 6 out of the 14 visited samples.

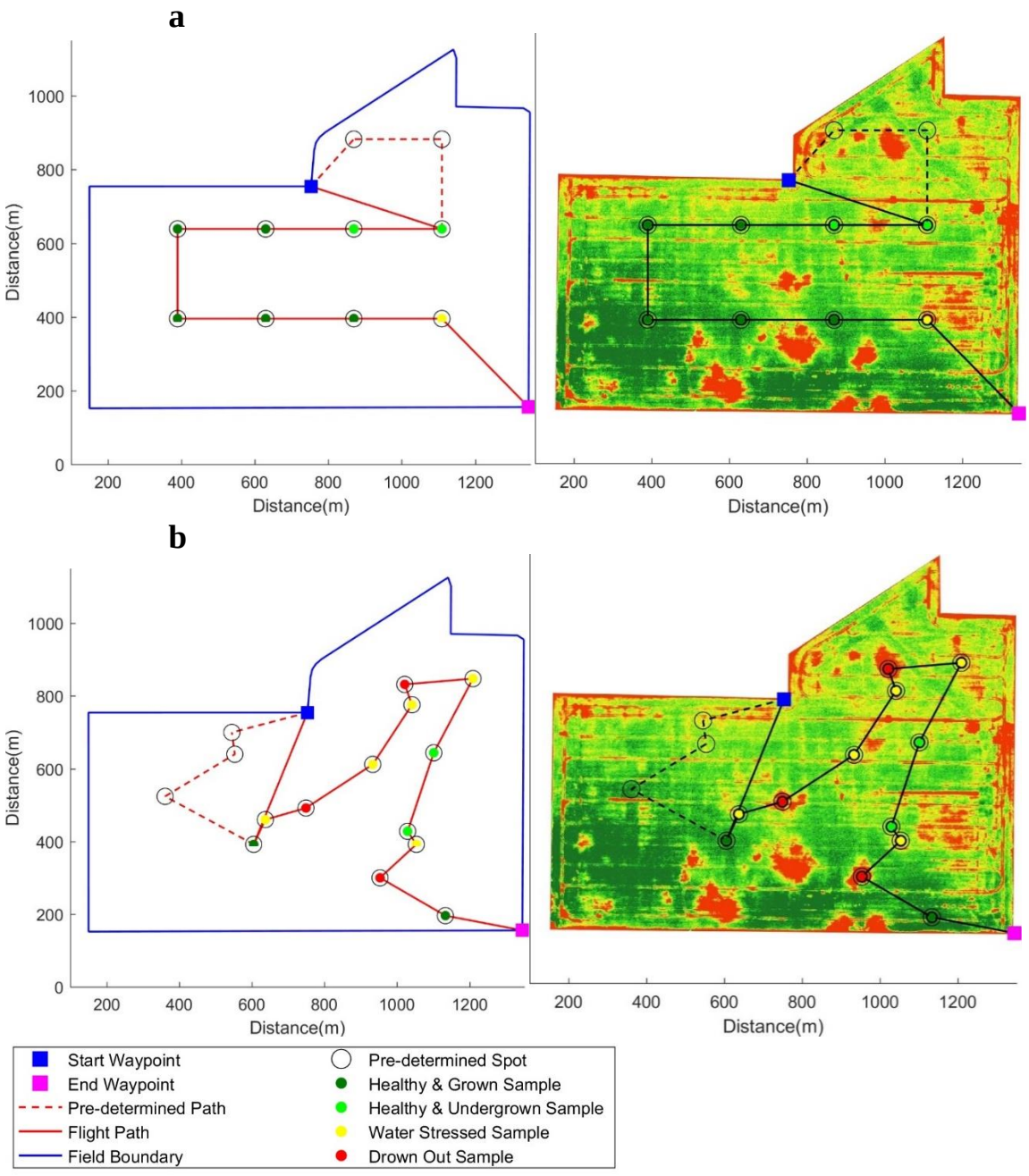

Figure 1-14. Conventional approach for Kossuth field through a) grid routing b) human expert routing for the V10S2Ws scenario

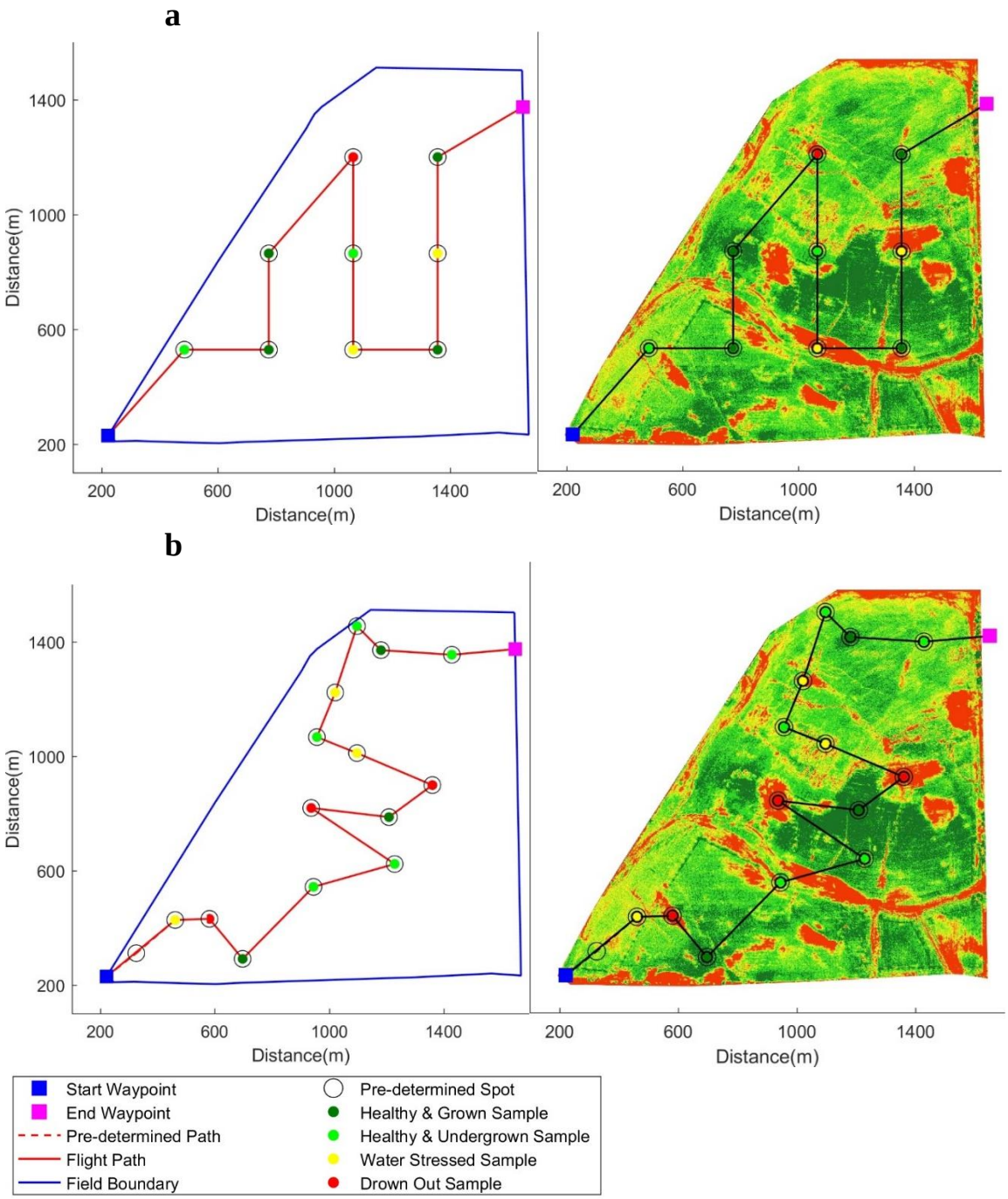

Figure 1-15. Conventional approach for Bremer field through a) grid routing b) human expert routing for the V15S3Wu scenario

Table 1-5 represents a comparison of the average results of the two approaches assumed to be employed by farmers, when the vehicle traveled at different velocities. Each component is the average of the 12 different scenarios, with different starting location and weight for the color zones. The human expert sampling significantly

outperformed the grid routing approach. The sample The human expert sampling consistently consumed the vehicle energy more efficiently to scout, as the number of visited samples significantly increased, by 43% on average, and less energy was retained at the end of missions. This method also made it possible to sample from every individual color zone of interest, and as such to achieve more comprehensive information with regard to the field condition.

Table 1-5. Average sampling properties in different velocities through the farmers' methods

Test Field	Velocity (m/s)	Grid Sampling					Human Expert Sampling				
		# of Samples	ASP	TSL	SD (%)	Remaining Energy (s)	# of Samples*	ASP	TSL*	SD (%)	Remaining Energy (s)
Kossuth	10	7	0.9	6.0	75	25	10 (43%)	0.96	9.2 (52%)	98	17
	15	10	0.9	9.1	75	262	14 (40%)	0.96	13.7 (50%)	100	241
Bremer	10	4	0.9	3.6	67	18	5 (25%)	0.96	4.7 (31%)	90	13
	15	9	0.9	8.3	100	38	12 (33%)	0.95	11.9 (43%)	100	26

* Numbers in percent quantify the percentile improvement by the human expert routing over the grid routing

1.4.4.2 Computational Approach

The computerized-based optimized sampling always outnumbered the farmers methods in sample selection (Table 1-6). The samples selected were highly representative of their corresponding color zones, i.e., having ASP approximately equal to 1.00. Additionally, the samples were selected from all color zones of interest, which provided a relatively thorough information as to the field condition. As demonstrated, in all of the scenarios for both Kossuth and Bremer fields, the remaining energy level were less than 5 s flight. This indicated the approach was highly efficient in terms of energy consumption, and ensured visiting more samples.

Table 1-6. Scouting results for all the scenarios through computation approach

Test Scenarios	Kossuth Field					Bremer Field				
	# of Samples	ASP	TSL	SD (%)	Remaining Energy (s)	# of Samples	ASP	TSL	SD (%)	Remaining Energy (s)
V10S1We	19	0.98	18.77	100	3	13	1.00	12.99	100	4
V10S1Wg	17	0.99	16.99	100	1	16	0.99	15.89	100	1
V10S1Wu	20	0.99	19.99	100	1	14	0.99	13.97	100	1
V10S1Ws	18	0.99	17.99	100	4	13	0.99	12.99	100	1
V10S2We	17	0.99	16.99	100	5	14	0.99	13.99	100	2
V10S2Wg	22	0.99	21.99	100	1	16	0.99	15.99	100	1
V10S2Wu	22	0.99	21.99	100	1	14	0.99	13.97	100	1
V10S2Ws	21	0.99	20.99	100	2	17	0.99	16.95	100	1
V10S3We	18	0.99	17.99	100	1	11	0.95	10.40	100	3
V10S3Wg	21	0.99	20.96	100	1	13	0.99	12.99	100	1
V10S3Wu	19	0.99	18.99	100	4	11	0.99	10.99	100	2
V10S3Ws	20	0.99	19.99	100	2	12	0.99	11.98	100	1
V15S1We	48	0.99	47.99	100	3	25	0.99	24.97	100	1
V15S1Wg	55	0.99	54.95	100	1	25	0.99	24.97	100	1
V15S1Wu	54	0.99	53.97	100	1	21	0.99	20.97	100	1
V15S1Ws	51	0.99	50.99	100	1	28	0.99	27.97	100	1
V15S2We	50	0.99	49.99	100	2	24	0.99	23.76	100	1
V15S2Wg	54	0.99	53.96	100	1	31	0.99	30.97	100	1
V15S2Wu	54	0.99	53.99	100	2	25	0.99	24.97	100	2
V15S2Ws	54	0.99	53.99	100	1	26	0.99	25.97	100	1
V15S3We	53	0.99	52.98	100	1	26	0.98	25.63	100	4
V15S3Wg	55	0.99	52.93	100	1	27	0.99	26.96	100	2
V15S3Wu	52	0.99	51.97	100	1	24	0.99	23.98	100	2
V15S3Ws	55	0.99	54.93	100	1	21	0.99	20.97	100	1

* V represents Velocity (m/s); S represents Start/Stop location; and W indicates which color zone is weighted as the highest (e indicates equal weight for all samples, and g, u, and s are associated with the healthy and grown, healthy and undergrown, and water stressed zones, respectively.

The TSL as an interesting and important parameter which quantifies how well sampling and routing performed was also improved (Figure 1-16 and Figure 1-17),

compared to the farmers' methods. The improvement stemmed from the increase in both the number of samples and the expressiveness of the samples. The magnitude of the TSL improvement varied based on the vehicle velocity. This was due to the direct impact of the number of samples on the TSL, which increased as the vehicle velocity increased (Table 1-7). The TSL change rate, however, was not dependent upon the vehicle velocity. For the Kossuth field, with the increase in velocity (from 10 to 15 m/s) the TSL improvement escalated as well (from 112% to 285% improvement, on average), whereas for the Bremer field this increase reduced the TSL improvement (from 189% to 112%, on average). This was expected as a multitude of causes affect the TSL change rate such as the distribution of color zones, the number of highly representative samples, and the size of a field.

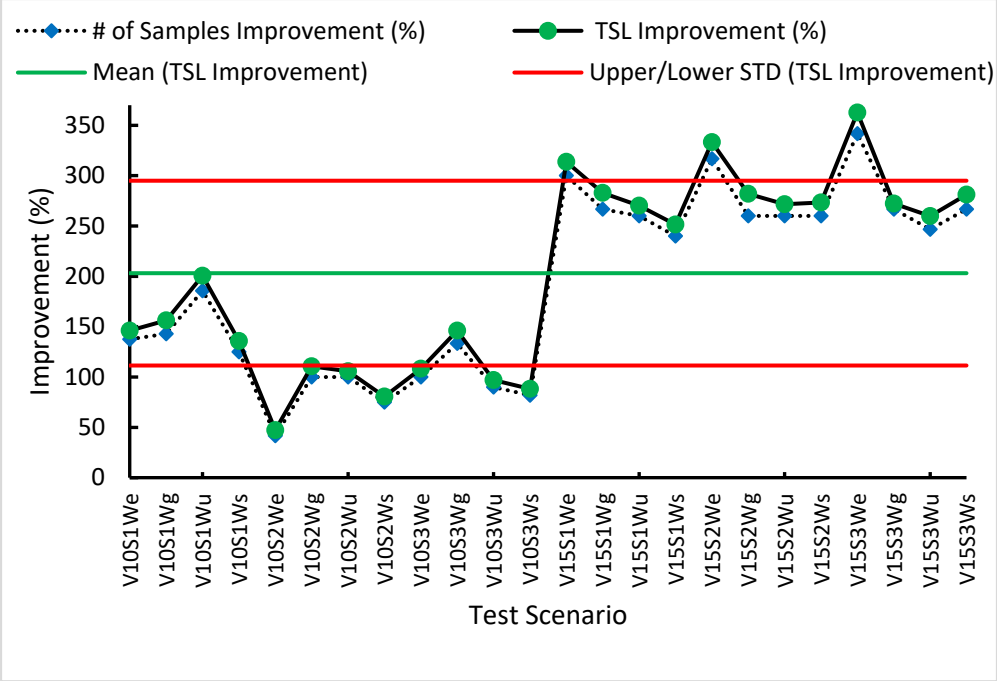

Figure 1-16. TSL improvement through computation compared to the HER, for the Kossuth field

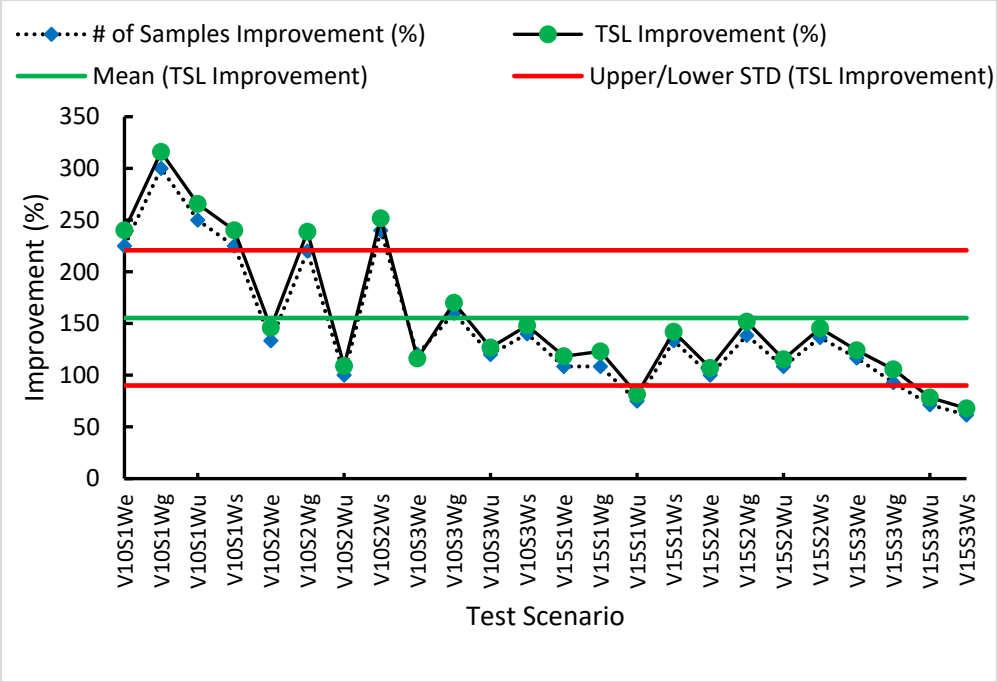

Figure 1-17. TSL improvement through computation compared to the HER, for the Bremer field

Table 1-7. Average sampling properties in different velocities through computational routing

Test Field	Velocity (m/s)	Human Expert Sampling					Computational Sampling				
		# of Samples	ASP	TSL	SD (%)	Remaining Energy (s)	# of Samples*	ASP	TSL*	SD (%)	Remaining Energy (s)
Kossuth	10	10	0.96	9.2	98	17	20 (100%)	0.99	19.5 (112%)	100	2
	15	14	0.96	13.7	100	241	53 (279%)	0.99	52.7 (285%)	100	1
Bremer	10	5	0.96	4.7	90	13	14 (180%)	0.99	13.6 (189%)	100	2
	15	12	0.95	11.9	100	26	25 (108%)	0.99	25.2 (112%)	100	2

* Numbers in percent quantify the percentile improvement using the computational routing

Figure 1-18 demonstrates the sampling and routing computed through the GA technique for the scenarios discussed on the Figure 1-16 and Figure 1-17. The improvements in the number of visited samples were predominantly arisen from the fact of reducing travel time. Unlike the human determined routing, the computerized generated routes avoided unnecessary deviations to visit more samples within the same time window as the farmers' methods. This approach attempted to travel over the nearest samples with the highest probability of being representative to the corresponding color zone. As such there were less meanderings in the route, which made it appear mostly similar to a straight path rather than a random-walk path created by the human expert.

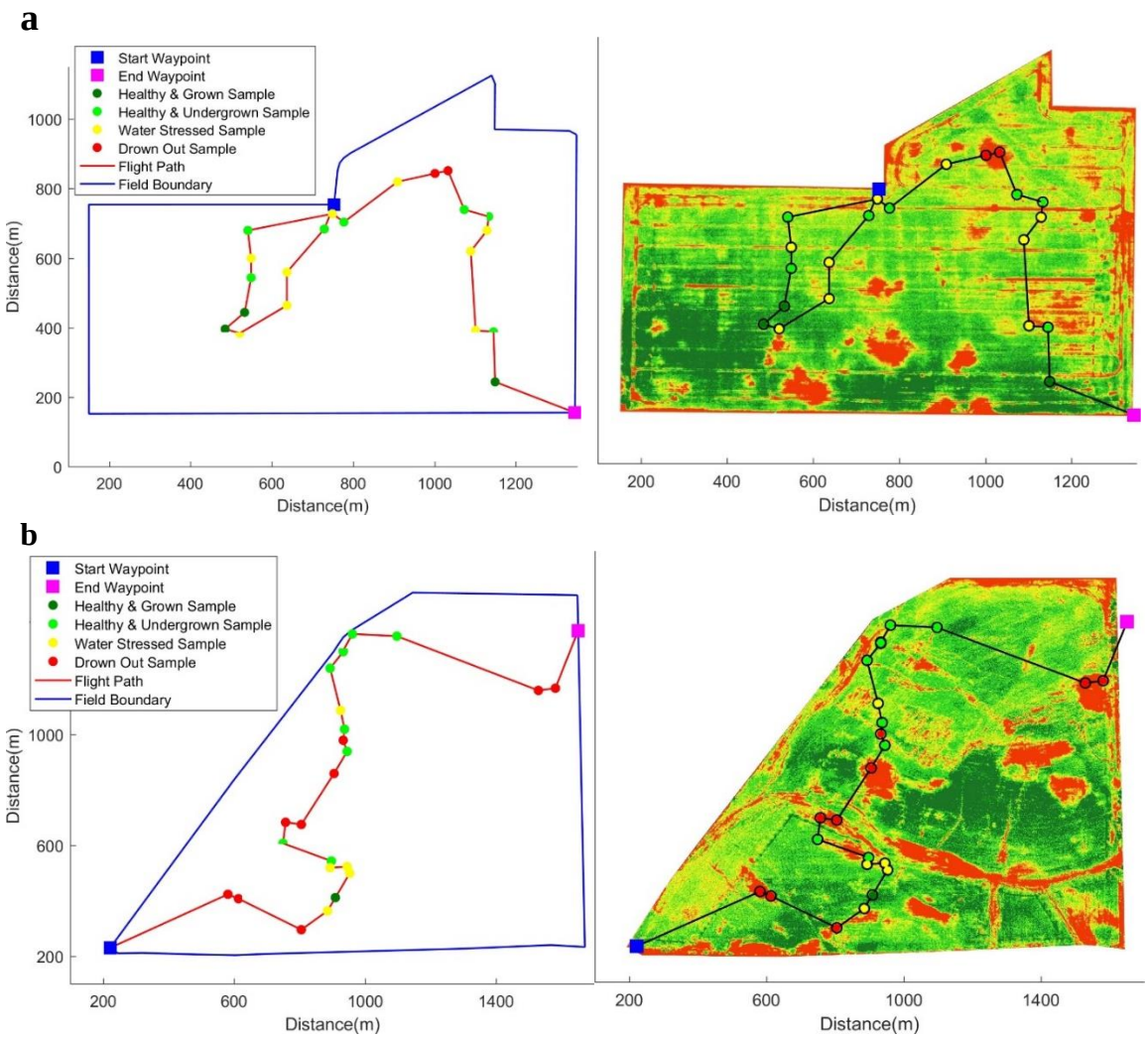

Figure 1-18. A representative example sampling and routing through the computational approach for a) Kossuth field (V10S2Ws scenario) and b) Bremer field (V15S3Wu scenario)

The local search characteristic of the GA technique allowed the consideration of a various number of samples at each iteration (Figure 1-19). The samples in each iteration were evaluated through the two separate fitness functions to ensure the maximization of the TSL and the minimization of the route which flies over the samples and then returns to the start location. The number of iterations in which the solution betterment took place varied according to the number of samples, the remaining energy, and the vehicle velocity.

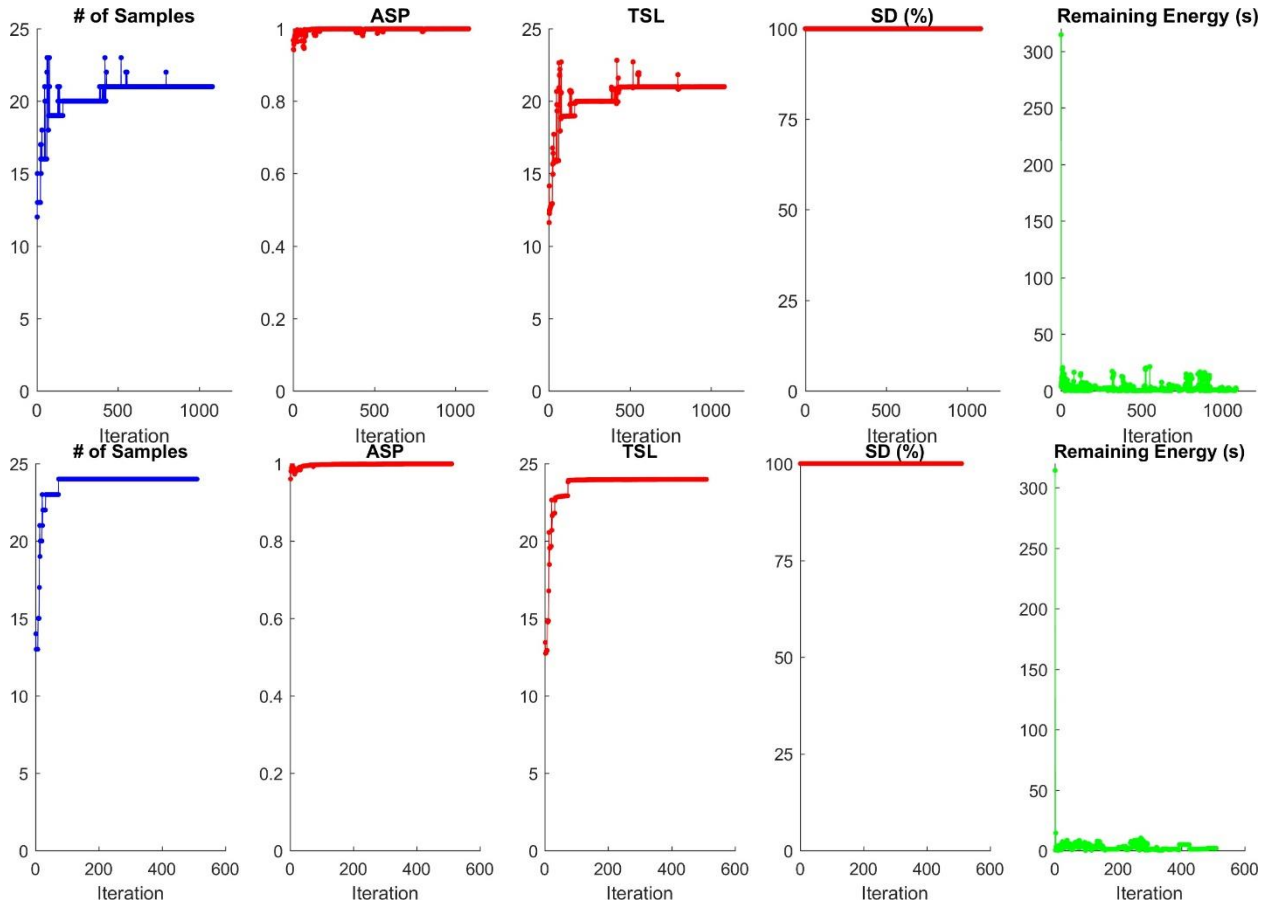

Figure 1-19. The improvement of the initial solution over iterations through the computational approach for a) Kossuth field (V10S2Ws scenario) and b) Bremer field (V15S3Wu scenario)

CHAPTER 2: CONCLUSION AND FUTURE WORK

2.1 CONCLUSIONS

This thesis proposes, and evaluates by simulation, a new approach for obtaining detailed and timely information about field condition. The approach centers on packing two conceptually separate flight plans into a single aerial survey conducted by a UAV.

To quickly obtain NDVI imagery for the entire field, the first flight plan begins at the UAV launch location and follows established paths to photograph the entire field at the maximum allowed altitude. The route taken is determined by a recursive nearest neighborhood algorithm ordering the established paths and taking into account the camera view coverage. The photogrammetry occurs at the highest altitude (set by the FAA at 400 feet) and velocity (determined by the particular UAV; for the DJI Mavic Pro, 15 m/s). Despite high velocity along an efficient route, a large fraction of the total permissible flight time is spent in this portion of the flight: 57% for an 86-hectar field and 87% for a 133-hectar field.

The second portion of the flight begins where the first part ended, and ends at the original UAV launch site. The goal of this second flight plan is to scout a set of representative points maximizing the quality of actionable information about the field condition. A zero-order, Takagi-Sugeno fuzzy logic model was employed to classify each point in the field using the NDVI imagery mapped into an HSV color space. The model performed accurately (was in agreement with human visual perception of colors) to distinguish a variety of discrete categories of field conditions that various zones of the field evidenced. Six zone types were distinguished, but over 86% of the fields were of four types with obvious significance: healthy and grown, healthy and undergrown, water stressed, and drown out. The fitness of potential flight plans for sampling representative points was judged based on a metric combining the new ASP and TSL quality measures. The scouting flight plan is thus created by a GA optimizing the choice of which points to visit, and the order in which to visit them, while still allowing the UAV to safely return to the launch site.

This new approach was evaluated by simulation and comparison with grid sampling and human expert sampling – competing approaches currently in use. A total of 48 scenarios were evaluated: all combinations of two fields, two different UAV

velocities, three different launch sites, and four different fitness weightings of relative zone importance. The ASP improved to be highly representative of the corresponding zones, being approximately 100%. The TSL also improved substantially, 50% to 350%, with an average up to 285% over field/velocity pairings.

2.2 FUTURE WORK

This extremely positive simulation result has not yet been confirmed by actual UAV flights, which would be the next step.

REFERENCES

Baboo, S. S., & S. Thirunavukkarasu (2014). "Image segmentation using high resolution multispectral satellite imagery implemented by FCM clustering techniques." *International Journal of Computer Science Issues (IJCSI)* 11(3): 154.

Bhatia, A., S. Srivastava, & A. Agarwal (2010). Face detection using fuzzy logic and skin color segmentation in images. *Emerging Trends in Engineering and Technology (ICETET), 2010 3rd International Conference on*, IEEE.

Bora, D. J., & A. K. Gupta (2014). "Clustering approach towards image segmentation: an analytical study." *arXiv preprint arXiv:1407.8121*.

Bruce, J., T. Balch, & M. Veloso (2000). Fast and inexpensive color image segmentation for interactive robots. *Intelligent Robots and Systems, 2000.(IROS 2000). Proceedings. 2000 IEEE/RSJ International Conference on*, IEEE.

Chaves-González, J. M., M. A. Vega-Rodríguez, J. A. Gómez-Pulido, & J. M. Sánchez-Pérez (2010). "Detecting skin in face recognition systems: A colour spaces study." *Digital Signal Processing* 20(3): 806-823.

Chen, J., T. N. Pappas, A. Mojsilovic, & B. E. Rogowitz (2005). "Adaptive perceptual color-texture image segmentation." *IEEE Transactions on Image Processing* 14(10): 1524-1536.

DJI, Company (2017). "Mavic Specs." from https://www.dji.com/mavic/info.

Dong, G., & M. Xie (2005). "Color clustering and learning for image segmentation based on neural networks." *IEEE transactions on neural networks* 16(4): 925-936.

Ehmke, T. (2013). "Unmanned aerial systems for field scouting and spraying." *Crops and Soils* 46(6): 4-9.

Freksa, C. (1994). "Fuzzy logic: An interface between logic and human reasoning." *IEEE Expert* 9(4): 20-21.

Ganesan, P., & V. Rajini (2014). YIQ color space based satellite image segmentation using modified FCM clustering and histogram equalization. *Advances in Electrical Engineering (ICAEE), 2014 International Conference on*, IEEE.

Goldberg, D. (1989). Genetic Algorithms in Search, Optimization, and Machine Learning, Addison Wesley, Reading, Massachusetts.

Hunt, E. R., M. Cavigelli, C. S. Daughtry, J. E. Mcmurtrey, & C. L. Walthall (2005). "Evaluation of digital photography from model aircraft for remote sensing of crop biomass and nitrogen status." *Precision Agriculture* 6(4): 359-378.

Inman, D., R. Khosla, R. Reich, & D. Westfall (2008). "Normalized difference vegetation index and soil color-based management zones in irrigated maize." *Agronomy journal* 100(1): 60-66.

Jain, R., R. Kasturi, & B. G. Schunck (1995). *Machine vision*, McGraw-Hill New York

Miller, J. O., J. Adkins, & K. Tully (2017). Providing Aerial Images through UAVs, University of Maryland. Fact Sheet, FS-1056.

Moreno-Cadenas, J. A., F. Gómez-Castañeda, A. Anzueto-Rios, & L. Hernández-Gómez (2016). Fuzzy inference system for region segmentation using the YCbCr color model. *Electrical Engineering, Computing Science and Automatic Control (CCE), 2016 13th International Conference on*, IEEE.

Peñuelas, J., J. Gamon, A. Fredeen, J. Merino, & C. Field (1994). "Reflectance indices associated with physiological changes in nitrogen-and water-limited sunflower leaves." *Remote sensing of Environment* 48(2): 135-146.

Pierpaoli, E., G. Carli, E. Pignatti, & M. Canavari (2013). "Drivers of precision agriculture technologies adoption: A literature review." *Procedia Technology* 8: 61-69.

Pujara, H., & K. M. Prasad (2013). "Image segmentation using learning vector quantization of artificial neural network." *Image* 2(7).

Sakamoto, T., A. A. Gitelson, A. L. Nguy-Robertson, T. J. Arkebauer, B. D. Wardlow, A. E. Suyker, S. B. Verma, & M. Shibayama (2012). "An alternative method using digital cameras for continuous monitoring of crop status." *Agricultural and forest meteorology* 154: 113-126.

Sathya, B., & R. Manavalan (2011). "Image segmentation by clustering methods: performance analysis." *International Journal of Computer Applications* 29(11).

Saxe, D., & R. Foulds (1996). Toward robust skin identification in video images. *Automatic Face and Gesture Recognition, 1996., Proceedings of the Second International Conference on*, IEEE.

Smith, A. R. (1978). "Color gamut transform pairs." *ACM Siggraph Computer Graphics* 12(3): 12-19.

Sobottka, K., & I. Pitas (1996). Face localization and facial feature extraction based on shape and color information. *Image Processing, 1996. Proceedings., International Conference on*, IEEE.

Sturm, B. L., & L. Daudet (2011). "Recursive nearest neighbor search in a sparse and multiscale domain for comparing audio signals." *Signal Processing* 91(12): 2836-2851.

Takagi, T., & M. Sugeno (1983). "Derivation of fuzzy control rules from human operator's control actions." *IFAC Proceedings Volumes* 16(13): 55-60.

Takagi, T., & M. Sugeno (1985). "Fuzzy identification of systems and its applications to modeling and control." *IEEE transactions on systems, man, and cybernetics*(1): 116-132.

Tominaga, Y. (1998). "Representative subset selection using genetic algorithms." *Chemometrics and Intelligent Laboratory Systems* 43(1): 157-163.

Tseng, D.-C., & C.-H. Chang (1992). Color segmentation using perceptual attributes. *Pattern Recognition, 1992. Vol. III. Conference C: Image, Speech and Signal Analysis, Proceedings., 11th IAPR International Conference on*, IEEE.

VanderLeest, Z., R. Bergman, M. Darr, & C. Murphy (2016). Choosing the Right Imagery: Best Management Practices for Color, NIR, and NDVI Imagery, Iowa State University Extension and Outreach.

Wharton, S. W., Y.-C. Lu, B. K. Quirk, L. R. Oleson, J. A. Newcomer, & F. M. Irani (1988). "The Land Analysis System (LAS) for multispectral image processing." *IEEE Transactions on Geoscience and Remote Sensing* 26(5): 693-697.

Wu, Y. T. (2000). "R2V: Automated Map Digitizing." *GIS Development* IV(12): 28-33.

Yang, C., J. H. Everitt, & J. M. Bradford (2006). "Comparison of QuickBird satellite imagery and airborne imagery for mapping grain sorghum yield patterns." *Precision Agriculture* 7(1): 33-44.

Yu, Z., Z. Cao, X. Wu, X. Bai, Y. Qin, W. Zhuo, Y. Xiao, X. Zhang, & H. Xue (2013). "Automatic image-based detection technology for two critical growth stages of maize: Emergence and three-leaf stage." *Agricultural and forest meteorology* 174: 65-84.

Zadeh, L. A. (1965). "Fuzzy sets." *Information and control* 8(3): 338-353.

Zhang, C., & J. M. Kovacs (2012). "The application of small unmanned aerial systems for precision agriculture: a review." *Precision Agriculture* 13(6): 693-712.

VITA

Hasan Seyyedhasani

EDUCATION

- M.S. Mechanical Engineering of Agricultural Machinery,
  University of Tehran, Tehran, Iran, November 2010, Advisor: Ali Jafari, Ph.D.
  Thesis: Design, Development, and Evaluation of Hydrostatic Drive for Traveling Mechanism on John Deere 1165 Combine Harvester. GPA: 3.45
- B.S. Mechanical Engineering of Agricultural Machinery, University of Tehran, Tehran, Iran, July 2006. Concentration: Electronic Control Unit (ECU). GPA: 3.03

PROFESSIONAL POSITIONS

- Graduate Research Assistant, Biosystems and Agricultural Engineering, University of Kentucky (December 2013- Present)
- Project Manager, Research and Development Department, Iran Combine Manufacturing Company * (ICM. Co.) (October 2008- November 2013)
- After Sales Services Department, ICM. Co. (November 2006-October 2008)
- Plastic Injection Molding Company (July 2005-January 2006)

FUNDED RESEARCH PROPOSAL

- **Seyyedhasani, H**., Jafari, A. 2009. Design, Development, and Evaluation of Hydrostatic Drive for Traveling Mechanism on JD 1165 Combine Harvester. $6,000, Mine and Industry Ministry, Under contract number: 450/51027041. Role: PI

SCHOLASTIC AND PROFESSIONAL HONORS

- Graduate Student Professional Travel Funding, $375 (March 2017), Awarded by the Gamma Sigma Delta, University of Kentucky Chapter.

---

* Affiliated with John Deere Company prior to 1982.

- Scientific Publication Scholarship Award, $500 (November 2016), Recognized contribution to Biosystems and Agricultural Engineering Department, University of Kentucky
- Research highlig**ht** (April 2015), Handheld Devices Provide Poor Location Accuracy, *Successful Farming*.
- Ranked in the top %1 (August 2008), Among all participants in the National Entrance Exam for M.S.
- Distinguished award of Exemption for Military Service (April 2005), Thanks to achieving second-rank at the Nationwide Entrance Exam of

PROFESSIONAL PUBLICATIONS

- **Seyyedhasani, H**., Dvorak, J.S. 2017. Using the Vehicle Routing Problem to Reduce Field Completion Times with Multiple Machines. Computers and Electronics in Agriculture, 134: 142-150.
- **Seyyedhasani, H**., Dvorak, J.S., Sama, M.P., Stombaugh, T.S. 2016. Mobile Device-Based Location Services Accuracy. Applied Engineering in Agriculture (ASABE), 32(5): 539-547.
- **Seyyedhasani, H**. 2017. Annual Operating Cost for Multiple Machines versus Single Machine. Agricultural Research & Technology: Open Access Journal, 4(4): 555643.
- **Seyyedhasani, H.,** Dvorak, J.S. Reducing Field Work Time Using Fleet Routing Optimization. Biosystems Engineering. "Under Review"
- Sarvandi, M., Najafizadeh, M., **Seyyedhasani, H**., Ehsanifar, M., and Hedayati, H. 2017. Non-Linear Response of Torsional Buckling Piezoelectric Cylindrical Shell Reinforced with DWBNNTs Under Combination of Electro-Thermo-Mechanical Loadings in Elastic Foundation. Chinese Journal of Mechanical Engineering. "In Press"
- **Hassani, H.S**., Jafari, A., Mohtasebi, S.S., and Setayesh, A.M. 2010. Transient Heat Transfer Analysis of Hydraulic System on JD 955 Harvester Combine by Finite Element Method. Journal of Food, Agriculture & Environment, 8(2): 382-385.

- **Hassani, H.S**., Jafari, A., Mohtasebi, S.S., and Setayesh, A.M. 2011. Fatigue Analysis of Hydraulic Pump Gears of JD 1165 Harvester Combine through Finite Element Method. Trends in Applied Science Research, 6(2): 174-181.
- **Hassani, H.S**., Jafari, A., Mohtasebi, S.S., and Setayesh, A.M. 2011. Hydraulic System of JD 955 Combine Harvester as Well as Presented Services Based on Statistical Analysis. Asian Journal of Agricultural Research, 5(1): 67-75.
- **Hassani, H.S**., Jafari, A., Mohtasebi, S.S., and Setayesh, A.M. 2011. Investigation on Grain Losses of the JD 1165 Combine Harvester Equipped with Variable Pulley and Belt for Forward Travel. American Journal of Food Technology, 6(4): 314-321.
- **Hassan, H.S**, Ali, J., Seyed, S., and Ali, M. 2010. Fatigue Analysis of Hydraulic Pump Gears of JD 955 Harvester through Finite Element Method. Journal of American Science, 6(7): 62-67.

PROFESSIONAL PRESENTATIONS

- **Seyyedhasani, H**., Sama, M., Dvorak, J.S. Aerial Validation of a Logistics Model for Area Coverage in Agriculture, ASABE Annual International Meeting, July 16-19th, 2017, Spokane, WA, As Speech. (Upcoming)
- **Seyyedhasani, H**., Dvorak, J.S. Comparison of Traditional Path Assignment for Multiple Vehicles with Computer Generated One in Agricultural Field Context, ASABE Annual International Meeting, July 17-19th, 2016, Orlando, FL, As Speech.
- Dvorak, J.S., **Seyyedhasani, H**. Simple Field Logistics Simulation Comparing Field Efficiencies and Field Capacities between Larger and Smaller Equipment, ASABE Annual International Meeting, July 17-19th, 2016, Orlando, FL.
- **Seyyedhasani, H**., Dvorak, J.S. Multi-Vehicle Path Planning and Coordination in Agricultural Fields, ASABE Annual International Meeting, July 26-29th, 2015, New Orleans, LA, As Speech.
- Javanshir, M**., Seyyedhasani, H**., Anajafi, S. Application of New Technologies in Agricultural Machinery, the 7th National Conference on Agricultural Machinery

Engineering & Mechanization, September 5-6th, 2012, Shirza University, Shiraz, Iran.

PROFESSIONAL RESEARCH PROJECTS

Biosystems and Agricultural Engineering Department

- Efficient Routing of Multiple Vehicles for Agricultural Area Coverage Tasks. (2015), Dvorak, J.S., Sama, M.P. $30,000, KSEF-3583-RDE-019. Role: Senior Personnel
- Location services (GPS, Network, Google Services) accuracy of mobile devices. (2014), USDA National Institute of Food and Agriculture (NIFA) Hatch Multistate project under 1001110. Role: Senior Personnel

Iran Combine Manufacturing Company

- Project Manager of Engine of 1055 Combine Harvester (2009-2013)
- Project Manager of Compressed Air Generation System (November 2013)
- Yield Monitoring System (December 2012)
- Project Manager of Brake and Clutch System (June 2012)
- ECU and GPS Systems (December 2011)
- Project Manager of Straw Chopper Machine (July 2011)
- Hydrostatic Drive for Traveling Mechanism (November 2010)
- Vibration Monitoring and Noise Emission (September 2010)
- Managed as Manager of Research and Development Department (March 2013-September 2013)

Private Sector

- Hydrostatic Drive Test for Propulsion (May 2012)

TEACHING EXPERIENCE

- Fluid Power Systems (BAE 515), Biosystems and Agricultural Engineering, University of Kentucky, Spring 2014 and 2015.
- Power Train, Engine, and Hydraulic Systems of JD 955 and 1165 combine harvesters, (2006-2008).

- Electrical, and Hydraulic Systems combine harvester of JD 1450 and SAMPO 3065L (2006-2008).
- Operation and Adjustment for JD 349 and 359 Balers, (2006-2008).
- Operation, adjustments, and service and maintenance of combine harvesters (2006-2008).

EXTENSION ACTIVITIES

Outreach Presentations and Workshops

Location (Province City)	Date	Audience	Topic	Program Period (days)
Qom Qom	February 2007	Farmers, Students, Agricultural Engineers & Experts	Operational* JD 955 Harvester	1
Ardabil Ardabil	March 2007	Farmers	Operational, Technical** JD 955 Harvester	3
North Khorasan Esfarayen	April 2007	Farmers, Students and Agricultural Engineers & Experts	Operational, Technical JD 955 Harvester, Balers	4
Khuzestan Lali	April 2007	Agricultural Engineers & Experts	Operational, Technical JD 1165 Harvesters	3
Esfahan Esfahan	May 2007	Agricultural Engineers & Experts	Operational JD 955, and JD 1165 Harvester	3
Lorestan Azna	May 2007	Farmers, Students and Agricultural Engineers & Experts	Operational JD 955 Harvester	1
Zanjan Zanjan	June 2007	Farmers and Students	Operational, Technical JD 955 Harvester	3
Lorestan Malayer	May 2007	Agricultural Engineers & Experts	Operational Balers	1
Fars Shiraz	June 2007	Agricultural Engineers & Experts	Technical SAMPO 3065L Harvester	2
Hamedan Bahar	August 2007	Farmers, Students and Agricultural Engineers & Experts	Operational JD 955 Harvester	1

ICM. Co	February 2008	JD 1165 Harvester customers in the last year (30 Persons)	Operational, Technical JD 1165 Harvester	4
ICM. Co	February 2008	JD 1165 Harvester customers in the other year (27 Persons)	Operational, Technical JD 1165 Harvester	4
Zanjan Zanjan	March 2008	Farmers and Students	Operational, Technical JD 955 Harvester	3
Ardabil Ardabil	March 2008	Farmers	Operational, Technical JD 955 Harvester	3
Sistan & Baluchestan Zabol	April 2008	Agricultural Engineers & Experts	Operational JD 955 Harvester	1
Sistan & Baluchestan Zahedan	April 2008	Farmers, Students and Agricultural Engineers & Experts	Operational, Technical JD 955 Harvester, and Balers	3
Esfahan Esfahan	April 2008	Farmers, Agricultural Engineers & Experts	Operational JD 955, and JD 1165 Harvester	3
Hamedan Hamedan	May 2008	Agricultural Engineers & Experts	Operational JD 955 Harvester	1
Chaharmahal & Bakhtiyari Shahr-e-Kord	May 2008	Farmers, Students	Operational JD 955 Harvester	2
Ardabil Parsabad	May 2008	Farmers, Students and Agricultural Engineers & Experts	Operational JD 955 Harvester	2
Hamedan Nahavand	June 2008	Farmers, Students and Agricultural Engineers & Experts	Operational JD 955 Harvester	1
Zanjan Zanjan	June 2008	Farmers, Students and Agricultural Engineers	Operational, Technical JD 955 Harvester	3
Fars Marvdasht	July 2008	Farmers	Operational, Technical JD 955 and JD 1165 Harvesters	3
ICM. Co	August 2008	After Sales Services Experts and Technician Serving Farmers	Operational, Technical JD 955 and JD 1165 Harvesters	2

* Denotes operation, adjustments, and service and maintenance training

** Indicates power train, engine, electrical, and hydraulic systems training

Exhibition Presentations

- The 8th international Exhibition of Agricultural Factors, Machinery & Mechanization, February 12-15th, 2013, Mashhad, Iran.
- Agrotech-Agropars, The 7th international Exhibition of Agricultural Machinery, Pesticides, Seeds and Water Supply, May 9-13th, 2011, Shiraz, Iran.
- Agrotech-Agropars, The 6th international Exhibition of Agricultural Machinery, Pesticides, Seeds and Water Supply, May 4-7th, 2010, Shiraz, Iran.
- Annual Exhibition of Agricultural Machinery and Related Industries, April 10-12th, 2008, Arak, Iran.

Individual Outreach

- Each customer of JD 1165 and SAMPO 3065L Combine Harvester

SERVICE

National

- Cloud Computing and Internet of Things in Agriculture Apps Session Reviewer/Moderator– Sponsored by Technical Community of Information, Technology, and Sensor Control Systems (ITSC-254), ASABE Annual International Meeting, 2017, Spokane, WA. (Upcoming)
- Big Data, Data Analysis, and Apps Session Reviewer/Moderator– Sponsored by Technical Community of Information, Technology, and Sensor Control Systems (ITSC-254), ASABE Annual International Meeting, 2016, Orlando, FL.
- ASABE Journals Reviewer, 2017
- 2017 Undergraduate Summer Research and Creativity Grants (SRG), University of Kentucky, 2017
- Science Alert Journals Reviewer, 2017
- ASABE MS-58 Agricultural Equipment Automation, 2015-Present
- ASABE ITSC-254 Emerging Information Systems, 2015-Present
- ASABE ITSC-353 Instrumentation and Controls, 2015-Present

Departmental

- Graduate Recruitment Team 2017
- Departmental Seminar Committee 2015-2016, Student Member
- Graduate Recruitment Weekend 2016
- Graduate Student Blog Team 2016

Corporate

- Fluid Power Team of the ICM. Co. Executive Member, 2007-2013
- Research and Development Representative in European Foundation for Quality Management (EFQM) Audit, 2009-2013
- Research and Development Representative in Technical Meetings with Overseas Suppliers and Customers, 2009-2013

PROFESSIONAL ORGANIZATIONS

- The Unmanned Systems Research Consortium (USRC), University of Kentucky, Student Member
- The American Society of Agricultural and Biological Engineering (ASABE), Member Since 2014
- The International Honor Society of Agriculture, Gamma Sigma Delta, Member
- Iranian Society of Agricultural Machinery Engineering and Mechanization (ISAMEM), Member
- Agricultural and Natural Resources Engineering Organization, Iran (ANREO), Member

PROFESSIONAL DEVELOPMENT

Professional Meetings Attended

- ASABE Agricultural Equipment Technology Conference. Louisville, KY, 2017.
- ASABE Annual International Meeting. Orlando, FL. 2016.
- ASABE Annual International Meeting. New Orleans, LA. 2015.
- ASABE Agricultural Equipment Technology Conference. Louisville, KY, 2015.

- The 8th international Exhibition of Agricultural Factors, Machinery & Mechanization, Mashhad, Iran, 2013.
- Agrotech-Agropars, The 7th international Exhibition of Agricultural Machinery, Pesticides, Seeds and Water Supply. Shiraz, Iran, 2011.
- Agrotech-Agropars, The 6th international Exhibition of Agricultural Machinery, Pesticides, Seeds and Water Supply. Shiraz, Iran, 2010.
- Annual Exhibition of Agricultural Machinery and Related Industries, April 10-12th, 2008, Arak, Iran.
- The 2ed National Conference on Agricultural Machinery Engineering, Tehran University, Tehran, Iran, 2005.

In-Service Training

- Microsoft Azure – Research Computing in the Cloud. University of Kentucky, February 2017.
- Grant-writing Basics: A Framework for Success. Workshop, University of Kentucky, November 2016.

Arranged by Iran Combine Manufacturing Company

- Iran Tractor Manufacturing Company (ITMC). Tabriz, Iran. September 2013.
- Kooshesh Radiator Company. Tehran Iran. June 2013
- Iran Tractor Manufacturing Company (ITMC). Tabriz, Iran. December 2012.
- Heavy Equipment Production Company (HEPCO). Arak, Iran. July 2012.
- Wagon Pars Company. Arak, Iran. July 2012.

Hasan Seyyedhasani

October 20, 2017